Integrated Cellular and Plasma Proteomics of Contrasting B-cell Cancers Reveals Common, Unique and Systemic Signatures*[S]

Harvey E. Johnston‡§, Matthew J. Carter‡, Kerry L. Cox‡, Melanie Dunscombe‡, Antigoni Manousopoulou§¶, Paul A. Townsend‖, Spiros D. Garbis§¶, and Mark S. Cragg‡**

Approximately 800,000 leukemia and lymphoma cases are diagnosed worldwide each year. Burkitt's lymphoma (BL) and chronic lymphocytic leukemia (CLL) are examples of contrasting B-cell cancers; BL is a highly aggressive lymphoid tumor, frequently affecting children, whereas CLL typically presents as an indolent, slow-progressing leukemia affecting the elderly. The B-cell-specific overexpression of the *myc* and *TCL1* oncogenes in mice induce spontaneous malignancies modeling BL and CLL, respectively. Quantitative mass spectrometry proteomics and isobaric labeling were employed to examine the biology underpinning contrasting Eμ-*myc* and Eμ-*TCL1* B-cell tumors. Additionally, the plasma proteome was evaluated using subproteome enrichment to interrogate biomarker emergence and the systemic effects of tumor burden. Over 10,000 proteins were identified (q<0.01) of which 8270 cellular and 2095 plasma proteins were quantitatively profiled. A common B-cell tumor signature of 695 overexpressed proteins highlighted ribosome biogenesis, cell-cycle promotion and chromosome segregation. Eμ-*myc* tumors overexpressed several methylating enzymes and underexpressed many cytoskeletal components. Eμ-*TCL1* tumors specifically overexpressed ER stress response proteins and signaling components in addition to both subunits of the interleukin-5 (IL5) receptor. IL5 treatment promoted Eμ-*TCL1* tumor proliferation, suggesting an amplification of IL5-induced AKT signaling by TCL1. Tumor plasma contained a substantial tumor lysis signature, most prominent in Eμ-*myc* plasma, whereas Eμ-*TCL1* plasma contained signatures of immune-response, inflammation and microenvironment interactions, with putative biomarkers in early-stage cancer. These findings provide a detailed characterization of contrasting B-cell tumor models, identifying common and specific tumor mechanisms. Integrated plasma proteomics allowed the dissection of a systemic response and a tumor lysis signature present in early- and late-stage cancers, respectively. Overall, this study suggests common B-cell cancer signatures exist and illustrates the potential of the further evaluation of B-cell cancer subtypes by integrative proteomics. ***Molecular & Cellular Proteomics 16: 10.1074/mcp.M116.063511, 386–406, 2017.***

Burkitt's lymphoma (BL)[1] and chronic lymphocytic leukemia (CLL) represent the extremes of B cell cancers; BL is highly aggressive and frequently affects children, whereas CLL typically presents as an indolent, slow-progressing leukemia in the elderly (1, 2).

BL is a hallmark myc-driven tumor; induced by chromosomal translocation of the transcription factor *myc* to immunoglobulin (Ig) enhancers (3). Myc influences ~15% of the genome, regulating processes such as cell proliferation, metabolism, adhesion, angiogenesis and de-differentiation (4–6). Such neoplastic-like traits make *myc* an aggressive oncogene, dysregulated or overexpressed in most cancers (7). Formal proof of its oncogenic properties were demonstrated when human myc was placed into the μ Ig heavy chain enhancer (Eμ) region of the mouse. These 'Eμ-*myc*' mice

From the ‡Antibody and Vaccine Group, Cancer Sciences Unit, Faculty of Medicine, General Hospital, University of Southampton, Southampton SO16 6YD, UK; §Centre for Proteomic Research, Institute for Life Sciences, University of Southampton, Highfield Campus, Southampton, SO17 1BJ, UK; ¶Clinical and Experimental Sciences Unit, Faculty of Medicine, University of Southampton, Southampton SO16 6YD, UK; ‖Molecular and Clinical Cancer Sciences, Paterson Building, Manchester Cancer Research Centre, Manchester Academic Health Science Centre, University of Manchester, Manchester, M20 4BX

Received August 27, 2016, and in revised form, December 19, 2016
Published, MCP Papers in Press, January 4, 2017, DOI 10.1074/mcp.M116.063511
Author contributions: Conceptualization: H.E.J., P.A.T., S.D.G., and M.S.C. Methodology: H.E.J. Validation: H.E.J. and M.J.C. Formal analysis: H.E.J. Investigation: H.E.J. Resources: H.E.J., M.D., K.L.C., A.M., and S.D.G. Writing – Original draft: H.E.J. and M.S.C. Writing – Review & Editing: H.E.J., M.S.C., and M.J.C. Visualization: H.E.J. Supervision: M.S.C., P.A.T., and S.D.G. Funding Acquisition: M.S.C., P.A.T., and H.E.J.

[1] The abbreviations used are: BL, Burkitt's lymphoma; CLL, Chronic lymphocytic leukaemia; DEP, Differentially expressed protein; Eμ, μ Ig heavy chain enhancer; Ig, Immunoglobulin; iTRAQ, Isobaric tags for relative and absolute quantitation; Rs, Regulation score (mean of $\log_2$(ratios)/(SD of $\log_2$(ratios) +1)); SEC, Size exclusion chromatography; SuPrE, Subproteome enrichment; TMT, Tandem mass tags; WT, Wild type.

produced high-penetrance lymphomas within around 100 days, recapitulating several molecular and pathological aspects of BL (3, 8–10).

In contrast, CLL is a relatively indolent B-cell cancer, presenting with a $CD5^+CD19^+$ leukemia (11, 12). Up to 90% of CLL cases express TCL1—a protein involved in lymphocyte development (13–15). *TCL1* is suggested to promote cell survival and proliferation by amplification of AKT phosphorylation, induced by growth factor-, cytokine- and B-cell receptor-induced PI3K signaling (16, 17). The Eμ-*TCL1* mouse, overexpressing TCL1 in B-cells again through the μ enhancer, was developed as a potential model of CLL (18). Eμ-*TCL1* mice recapitulate the expanded bone marrow, splenic and circulatory $CD5^+$ B-cell populations of CLL, detectable from around 3–5 months of age. The disease progresses to lethal splenomegaly and leukemia at ~12 months (18, 19). Currently it is regarded as one of the most useful preclinical models of CLL (20, 21).

Together, these models provide the opportunity to study oncogenesis mediated by two contrasting oncogenes at opposing ends of the proliferative spectrum. Eμ-*myc* tumors, like BL, are highly aggressive, have rapid onset and form lymphoid tumors, whereas Eμ-*TCL1* mice, like CLL, present a relatively indolent and slow-developing leukemia with secondary lymphoid organ involvement (3, 18).

In addition to cellular characterizations of tumors, plasma analysis holds the potential to identify additional biological signatures arising during oncogenesis. In particular, extracellular fluids can provide insight into the tumor-host dialogue between the immune system and micro-environment and report on the metabolic and homeostatic aberrations that tumors display. Further, combining cellular and plasma characterization can provide greater insight into the mechanisms by which any biomarkers of disease may be entering the circulation.

Liquid chromatography coupled with mass spectrometry (LC-MS) proteomics currently provides the best means of establishing global differential protein expression profiles of cellular and plasma samples. These approaches are evolving rapidly and yielding ever-increasing proteome coverage (22, 23). Nonetheless plasma/serum proteomics still presents significant challenges because of the vast dynamic range of protein concentrations (24). Although advances continue to be made with immunodepletion strategies (25–27), an alternative method termed, Subproteome Enrichment by Size Exclusion Chromatography (SuPrE-SEC), offers an effective alternative. SuPrE-SEC uses size-dependent protein fractionation to deplete high-abundance proteins and enrich for low-abundance proteins. The resulting reduction of the protein concentration dynamic range facilitates a greater depth of LC-MS proteomics coverage (28, 29).

This investigation has applied multiplexed, LC-MS proteomics to the characterization of plasma subproteomes and isolated B-cell material from Eμ-*myc*, Eμ-*TCL1* and wildtype (WT) mice. The resulting proteomes have been interrogated to identify common and tumor-specific signatures and to understand the combined cellular and extracellular characteristics of B-cell tumors.

MATERIALS AND METHODS

Materials—Tris(hydroxymethyl)aminomethane (TRIS), SDS, Na_2EDTA, NH_4Cl, $NaHCO_3$, sodium deoxycholate (DOC), guanidine hydrochloride, glycine, HPLC and LC-MS grade ACN and formic acid (FA) and 100 μm cell sieves were purchased from Fisher Scientific, Loughborough, UK. Tween20 (tween), sodium heparin, propidium iodide (PI), carboxyfluorescein succinimidyl ester (CFSE), asparagine, 2-mercaptoethanol, octylphenoxypolyethoxyethanol (IgePalCA^{630}), triton x-100, protease inhibitors, ponceau S, acetic acid, methyl methanethiosulfonate (MMTS), tris(2-carboxyethyl)phosphine (TCEP), triethylammonium bicarbonate (TEAB), DMSO, hydroxylamine and ammonium hydroxide (NH_4OH) were purchased from Sigma, St. Louis, MO.

Dulbecco's modified Eagle's medium (DMEM), glutamine, pyruvate, penicillin and streptomycin were purchased from Life Technologies, Carlsbad, CA. Mouse B-cell isolation kits and magnetic cell sorting columns were purchased from Miltenyi Biotech, Bergisch Gladbach, Germany. Twenty-three-gauge needles and 1-ml syringes were purchased from BD Biosciences, Franklin Lakes, NJ, Interleukin 5 (IL5) recombinant protein from Peprotech, Rocky Hill, NJ, Immobilon 0.45 μm pore PVDF membrane from Millipore, Billerica, MA and nonfat milk from Marvel, Birmingham, UK. 30× DTT and 3× red loading buffer were purchased for Cell Signaling Technologies, Danvers, MA. Enhanced chemiluminescence reagents, tandem mass tags (TMT) 10-plex isobaric labeling reagents and 2 kDa M_w cut-off Slide-A-Lyzer dialysis cassettes and proteomics grade lys-c were purchased from Thermo Scientific, Waltham, MA. Proteomics grade trypsin was purchased from Roche, Basel, Switzerland. Isobaric tags for relative and absolute quantitation (iTRAQ) 8-plex reagents were purchased from ABSciex, Framingham, MA. Antibodies are detailed in Supplementary Methods.

Animals—Mice were bred and maintained in-house with procedures carried out in accordance with home office licenses PPL30/2450 and 30/2970 and PIL30/9925. Female Eμ-*myc* [C57BL/6J-TgN(Igh*myc*)22Bri/J] hemizygous and Eμ-*TCL1* [C57BL/6J-TgN(Igh*TCL1*)22Bri/J] hemizygous mice were used. The Eμ-*myc* and Eμ-*TCL1* transgenes were detected with PCR. Eμ-*myc* primers (annealing temperature; 55 °C): 5′- CAG CTG GCG TAA TAG CGA AGA G -3′ and 5′- CTG TGA CTG GTG AGT ACT CAA CC -3′ ~900 bp product, Eμ-*TCL1* primers (annealing temperature; 58 °C): 5′- GCC GAG TGC CCG ACA CTC -3′ and 5′- CAT CTG GCA GCT CGA -3′ ~250 bp product. Eμ-*TCL1* mice were screened monthly for count and percentage of $B220^+$ $CD5^+$ B-cells in the blood, being considered terminal either with >80% leukemic cells or palpated splenomegaly >3 cm. Eμ-*myc* mice

were checked daily and were considered terminal, typically upon visible lymph node tumor presentation.

Experimental Design and Statistical Rationale—Sample pooling, detailed in supplemental Figs. S1, was used to accommodate comparative experiments in single isobaric label sets. Tumorous spleens were collected from 4 Eμ-*myc* and 4 Eμ-*TCL1* mice with terminal tumor presentation. For nontumor controls, 6 spleens, handled as two pools of 3 spleens, were collected from 6 week old and 200 day WT littermates and 6 week-old Eμ-*myc* and Eμ-*TCL1* mice with no signs of tumor or splenomegaly (summarized in supplemental Fig. S1). Nontumor pools were analyzed with six samples per isobaric label, whereas tumor samples were analyzed as biological replicate pools of two tumors.

For plasma, six samples were individually collected for each of the above tumor and nontumor conditions, in parallel with B-cell isolation. In addition, 6 samples were isolated from Eμ-*TCL1* mice at a preterminal "30%" stage, when 30% $B220^+$ $CD5^+$ cells were present in the blood. To minimize bias these were selected from a cohort of 14 Eμ-*TCL1* mice, from every other mouse reaching the 30% threshold. Tumor and preterminal "30%" tumor plasma were also analyzed as biological replicates, with three samples allocated to each label.

Each pair of tumor pools was compared with two WT sample pools, generating four ratios which could be evaluated for consistency and significance to ensure the reproducibility of quantitative results. Replicate ratios were analyzed for consistency with an FDR-corrected *t* test and considered significant with a *p* value of <0.05. *p* values were coupled with a measure of magnitude detailed in Quantitative and Statistical Analysis of MS Data, below.

B-cell Isolation—B-cells were isolated from single-cell suspensions using the mouse negative selection B-cell isolation kits and MACS columns according to the manufacturer's instructions, washed once at room temperature (RT) in red blood cell lysis buffer (155 mM NH_4CL, 10 mM $NaHCO_3$, 0.1 mM Na_2EDTA (pH 7.4) before three washes in PBS. B-cell isolation efficiency was assessed by flow cytometry immunostaining with CD19 and CD3, typically yielding >90% purity with less than 2% T-cell ($CD3^+$) contamination (supplemental Fig. S1). B-cell pellets were snap frozen and stored in liquid nitrogen prior to lysate preparation.

Plasma Isolation—To isolate plasma, maximize sample purity, minimize red blood cell lysis and accommodate for organ displacement from tumors, an adaption of bleeding from the inferior vena cava under terminal anesthesia (30) was utilized. Using a 23-gauge needle, 700–1000 μl of blood was collected for each animal into 50 μg/ml sodium heparin in PBS. Blood was immediately placed on ice and centrifuged at 2000 $\times$ *g* for 15 min at 4 °C with plasma stored in liquid nitrogen. Samples were rejected if red blood cell lysis was visible by eye.

Plasma Subproteome Enrichment—20 μl was taken from each of the six replicate plasma samples described above to give pools of 120 μl. For tumor samples, two 120 μl pools of 3 $\times$ 40 μl were formed to provide biological replicates (summarized in Figs. 1 and supplemental Fig. S1).

SuPrE-SEC was adapted from that described previously (28). Each 120 μl plasma pool was diluted with 380 μl of 6 M guanidine hydrochloride in 10% methanol and separated by 3 KW804 SEC columns in series at 1.2 ml/min and 30 °C. The low molecular weight subproteome was isolated during elution from 42–55 min (Supplemental Fig. S1*G*) and dialyzed (2 kDa M_w cut-off) into ultrapure water (18.2 MΩ cm^{-1}) with five exchanges into 5 liters. Protein was lyophilized and re-solubilized in 0.5 M TEAB with 0.05% SDS with 30 μg digested and labeled for MS analysis as described below.

Sample Preparation for MS—Snap frozen cell pellets were lysed on ice by trituration with a 23-gauge needle in 0.5 M TEAB with 0.05% SDS. Disrupted cells were further sonicated and lysates cleared at 16,000 $\times$ *g* for 10 min at 4 °C. 100 μg of cell lysate or 30 μg of plasma subproteome was reduced with 50 mM TCEP and alkylated with 200 mM MMTS, before digestion overnight at RT with a 30:1 ratio of proteomics grade trypsin. Plasma proteins were additionally digested for a further 2 h at 37 °C with 100:1 proteomics grade Lys-c. Peptides were incubated with either iTRAQ 8-plex (B-cell peptides) or TMT 10-plex isobaric tags (plasma peptides) according to the manufacturer's instructions. Samples were then lyophilized and labeled peptides serially reconstituted, for each proteome, in 100 μl of 2% v/v ACN, 0.1% v/v NH_4OH.

Peptide Prefractionation—Peptides were resolved using high-pH (0.1% v/v NH_4OH) RP C8 chromatography (150 mm $\times$ 3 mm ID $\times$ 3.5 μm particle, XBridge, Waters, Milford, MA) at 300 μl/min with a LC-20AD HPLC system (Shimadzu) maintained at 30 °C, using the mobile phases (MP); A - 99.9% H_2O, 0.1% NH_4OH, B - 99.9% ACN, 0.1% NH_4OH. The 2 h gradient was as follows; 0 min; 2% B, 10 min; 2% B, 75 min; 30% B, 105 min; 85% B, 120 min; 2% B. Fractions were collected in a peak-dependent manner and lyophilized.

Peptide Fraction Resolution and Characterization by LC-MS/MS—Lyophilized peptide fractions were individually reconstituted in 2% ACN, 0.1% FA, and ~500 ng of peptides were subjected to nano-ultra-performance liquid chromatography by a Dionex Ultimate 3000 (Thermo Scientific). Conditions used varied between the plasma and B-cell proteomes, detailed in Supplementary Methods. In summary, peptides were trapped by C18 and eluted over a reverse phase gradient, of which several lengths were used depending on the peptide fraction abundance and proteome. The total MS time for the iTRAQ-labeled B-cell proteome was ~200 h, with the TMT-labeled plasma proteome analyzed over ~250 h.

Peptide elution was directly coupled to electrospray ionization at 2.4 kV using a PicoTip nESI emitter (New Objective, Woburn, Massachusetts), and were characterized with an

Orbitrap Elite Velos Pro mass spectrometer (Thermo Scientific). MS characterization of eluting peptides was conducted between 350 and 1900 m/z at 120,000 mass resolution. The top 12 + 2 and +3 precursor ions per MS scan (minimum intensity 1000) were characterized by tandem MS with high-energy collisional dissociation (HCD) (30,000 mass resolution (15,000 for the B-cell proteome), 1.2 Da isolation window, 40 keV normalized collision energy) and CID (ion trap MS, 2 Da isolation window, 35 keV). Additionally, the DMSO ion at 401.922718 was used as a MS lockmass (31).

MS Data Processing—Target-decoy searching of raw spectra data was performed with Proteome Discoverer software version 1.4.1.14 (Thermo Scientific). Spectra were subject to a two stage search, both using SequestHT (version 1.1.1.11), with Percolator used to estimate FDR with a threshold of $q \leq 0.01$. The first allowed only a single missed cleavage, minimum peptide length of 7, precursor mass tolerance of 5 ppm, no variable modifications and searched against the mouse UniProt Swissprot database, supplemented with the human sequences for (downloaded 01/15, 16,676 protein sequences). The second search used only spectra with $q > 0.01$ from the first search, allowed two missed cleavages, minimum peptide length of 6, searched against the human/mouse UniProt trembl database (with human myc and TCL1, downloaded 01/15, 52,469 protein sequences), precursor mass tolerance of 10 ppm and a maximum of two variable (1 equal) modifications of; TMT or iTRAQ (Tyr), oxidation (Met), deamidation (Asn, Gln) or phospho (Ser, Thr, Tyr). In both searches, fragment ion mass tolerances of 0.02 Da and 0.5 Da were used for HCD and CID spectra, respectively. Fixed modifications of Methythio (Cys), TMT or iTRAQ (Lys and N terminus) were used. PhosphoRS was used to predict the probability of specific phosphorylated residues. Reporter ion intensities were extracted from nonredundant PSMs with a tolerance of 20 ppm. To reduce ratio compression, peptide spectrum match data for proteins ($q<0.01$) were exported from Proteome Discoverer and submitted to Statistical Processing for Isobaric Quantitation Evaluation (SPIQuE) at spiquetool-.com. This method weighted the contributions of each PSM quantitation to a protein's quantitation on the basis of PSM features (manuscript in preparation). For example, high-intensity peptides with low isolation interference were given a greater weighting factor. Although the effects upon the ratios were minimal, the overall trend demonstrated efficient ratio decompression (Supplementary Methods). An example of the effect on the ratio decompression to the human TCL1 protein, discretely expressed in Eμ-*TCL1* B-cells, is outlined in Supplementary Methods.

The raw data and processed outputs have been deposited to the ProteomeXchange Consortium (32) via the PRIDE partner repository with the data set identifier PXD004608.

Quantitative and Statistical Analysis of MS Data—Log_2 (ratios) were generated describing each sample pool relative to the two WT controls. To define those proteins with the greatest fold change for each biological state, an FDR-corrected one sample *t* test was performed and average values determined. To derive a single, robust measure, representative of both the magnitude and consistency of differential expression, a ratio was defined between that of the mean and the standard deviation of the 4 log_2 ratios, termed the regulation score (Rs = mean/(standard deviation +1)). For proteins with no, or inconsistent differential expression, the Rs tends toward 0. The Rs also correlated more strongly with *p* values for each set of ratios (Supplementary Methods). In all instances, differentially expressed proteins (DEPs) were defined as those with an FDR-corrected *p* value of <0.05 and an Rs threshold of >0.5 or <-0.5. Although arbitrary, evaluation of this threshold demonstrated a minimum average fold change of 1.4, for which a fold change variation of just 6% was observed. This therefore fulfilled the power analysis principles described by Levin, 2011 (33), but on a case-by-case basis, by incorporating variation into each Rs via the S.D. as a denominator. The outliers for this threshold were additionally highlighted to demonstrate that consistent differential expression was still observed (Supplementary Methods). Other *p* values were determined by a false discovery rate-corrected 1- or 2-sample, two tailed, *t* test with no assumption of equal variance.

Bioinformatics Analyses—Proteins reaching the thresholds outlined above were submitted to either Ingenuity Pathway Analysis (IPA) or Database for Annotation, Visualization and Integrated Discovery (DAVID). For DAVID analyses, the default settings were used for pathway and gene ontology (GO) term enrichment, with Benjamini-corrected *p* values of <0.05 considered significant. For B-cell/tumor proteome enrichments, all quantified proteins were used as a background. For IPA analyses, default settings were used. Upstream regulator analysis was determined using all DEPs ($Rs>0.5/<-0.5$, $p < 0.05$). Annotations of biomarkers and drug targets were conducted by IPA. Plasma protein deconvolution was conducted by removing any proteins annotated by IPA as predominantly cellular in addition to any proteins with more than 30 PSMs from the B-cell proteome.

SDS-PAGE and Western blotting—Cells were lysed in radioimmunoprecipitation assay (RIPA) cell lysis buffer (0.15 M NaCl, 1% v/v octylphenoxypolyethoxyethanol (IgePalCA630), 0.5% w/v sodium deoxycholate (DOC), 0.1% w/v sodium dodecyl sulfate (SDS), 0.05 M TRIS (pH 8) and 1% v/v protease inhibitor) and as described previously (34). Lysate supernatants were isolated by centrifugation (16,000 × *g* for 10 min at 4 °C). Protein concentrations were determined by Bradford assay. Lysates were reduced in loading buffer with 2-mercaptoethanol at 95 °C for 5 min. Lysates were resolved by SDS-PAGE and transferred to PVDF. Membranes were blocked in 5% (w/v) nonfat milk for 1 h before probing with primary antibodies, as detailed in Supplementary Methods. Expression was detected by incubation with a horseradish peroxidase-conjugated secondary antibody using enhanced chemiluminescence reagents and a ChemiDoc-It imaging system

(UVP). GAPDH or tubulin were used as loading controls. Relative quantification of protein band intensity was determined using Image J, normalized against loading controls and ratios to WT B-cell lysates were derived. For Eμ-*myc* tumor validations, lysate protein concentrations were determined by bicinchoninic acid assay (BCA), reduced with DDT and diluted in 3x loading buffer. Western blots were visualized with fluorescent antibodies and an Odyssey Imaging System (Li-cor) and quantified using Image Studio 2.0 (Li-cor).

Cell Culture—Cells derived from Eμ-*myc* or Eμ-*TCL1* tumors were cultured in DMEM supplemented with 2 mM glutamine, 1 mM pyruvate, 45 units/ml penicillin, 45 μl/ml streptomycin, 200 μM asparagine, 50 μM 2-mercaptoethanol, and 10% FCS. Eμ-*myc* tumors were cultured a density of 5×10^7 cells/ml at 37 °C in 10% CO_2. Eμ-*TCL1* cells were cultured at a density of 5×10^6 cells/ml at 37 °C in 5% CO_2. Cells were cultured for 24 h prior to treatment. Serum starvation was conducted for 4 h in the above media with 0.5% BSA replacing FCS.

Flow Cytometry—Cells were stained with either the manufacturer's recommended concentration, or 10 μg/ml, of antibody (Supplementary Methods) for 30 min in the dark, washed and analyzed by flow cytometry with a FACScan or FACScalibur (BD) (35, 36). Relative expression was determined using the geometric means. Cell cycle status was assessed by hypotonic PI (50 μg/ml PI, 0.1% w/v sodium citrate, 0.1% w/v triton x-100) incubated at 4 °C for 15 min. PI fluorescence was measured by FL2 on a linear scale at the lowest flow rate. Cell division was tracked by CFSE dilution of cells stained with a concentration of 5 μM for 15 min at room temperature.

RESULTS

Quantitative Proteomics of Eμ-myc and Eμ-TCL1 Tumors and Plasma—To characterize the global proteome expression of Eμ-*myc* and Eμ-*TCL1* tumors, an 8-plex iTRAQ experiment was designed incorporating terminal tumor, premalignant and age-matched WT B-cells (Fig. 1). Sample pooling in combination with biological replicates enabled the averaging of biological variability of several samples within a single isobaric tag experiment. Splenic tumors samples, because of a greater anticipated variability, were pooled in two pairs of two tumors from each model; derived from a total of 8 terminal mice (supplemental Fig. S1). Nontumor controls consisted of samples pooled from six animals. For plasma proteomics, controls were again characterized as pools of six samples, with two pools of three plasma samples for each tumor condition. Additionally, plasma from preterminal Eμ-*TCL1* tumors was analyzed, derived from mice reaching a $CD5^+$ $B220^+$ leukemia threshold of 30%, termed "30%" samples. To accommodate these additional samples, TMT 10-plex isobaric labels were used.

The tumors selected for proteomics analysis, detailed in supplemental Fig. S1*A*–S1*F*, were representative of the range of characteristics observed for the model. The median terminal presentations, for example (supplemental Fig. S1*A*), of 92 and 318 days for Eμ-*myc* and Eμ-*TCL1* tumors, respectively, agreed with earlier reports (3, 8, 18, 19).

Splenic B-cells from tumors and controls were lysed, trypsin digested, and assigned to the eight isobaric labels of iTRAQ 8-plex (Fig. 1) to provide relative protein expression quantitation. The labeled B-cell peptides were pooled and characterized by two-dimensional (2D) LC-MS identifying 9260 proteins ($q<0.01$). 8270 proteins were relatively quantitated across all eight sample pools. The depth of proteome coverage and quantitation is summarized in supplemental Fig. S1*H*.

Plasma samples were subjected to an adapted form of SuPrE-SEC (28), reducing the dynamic range and facilitating deeper proteome coverage by the exclusion of the majority of high-abundant proteins (supplemental Table S1, supplemental Fig. S1*G*). 2D LC-MS characterization of the plasma subproteome provided relative quantitation for 2095 of the 2688 identified proteins ($q<0.01$). Peptide spectrum matches (PSMs) to the higher-M_w protein albumin ($n = 3835$, $M_w = 68.7$kDa), for example, were of far lower abundance than transthyretin ($n = 7769$, $M_w = 15.8$kDa) or apolipoprotein A-II ($n = 7129$, $M_w = 11.3$kDa). Given approximate plasma concentrations of 40 mg/ml, 260 μg/ml and 300 μg/ml for these proteins (37), respectively, this represented around a 275-fold enrichment of low M_w proteins.

Reproducibility and Validation of Quantitative Proteomics Results—The relative quantitative proteomes demonstrated tumor-dependent hierarchical clustering identifying common trends of differential tumor expression compared with both WT controls (Fig. 2*A*). Evaluation of the reproducibility between tumor sample pools by linear regression highlighted the strong correlation between the 5 pairs of independent biological replicates (Fig. 2*B*). Additionally, an overlap of 1288 proteins were quantitated in both the B-cell and plasma proteomes.

Individual protein expression was considered for a number of candidates to confirm the successful characterization and analysis of the quantitative proteome. The results presented an anticipated model-specific overexpression of the *myc* and *TCL1* human transgenes (Fig. 2*C*, supplemental Fig. S2*A*, S2*B*), in addition to characteristic CD5 overexpression and B220 underexpression for Eμ-*TCL1* tumors. Several DEPs were validated by antibody-based methods to further verify the relative quantitative accuracy of the proteomics; 10 for Eμ-*myc* tumors and 7 for Eμ-*TCL1* tumors (supplemental Fig. S2*G*, S2*H*). The $\log_2$ ratios to WT of these validations were plotted alongside the quantitative proteomics results (Fig. 2*D*). Additionally, previously reported DEPs in Eμ-*myc* or Eμ-*TCL1* tumors were compared with the proteomics results (supplemental Fig. S2*D*, S2*F*). A correlation was also observed with a study describing relative mRNA expression in Eμ-*myc* tumors (38) (supplemental Fig. S2*J*). Overall, the quantitative pro-

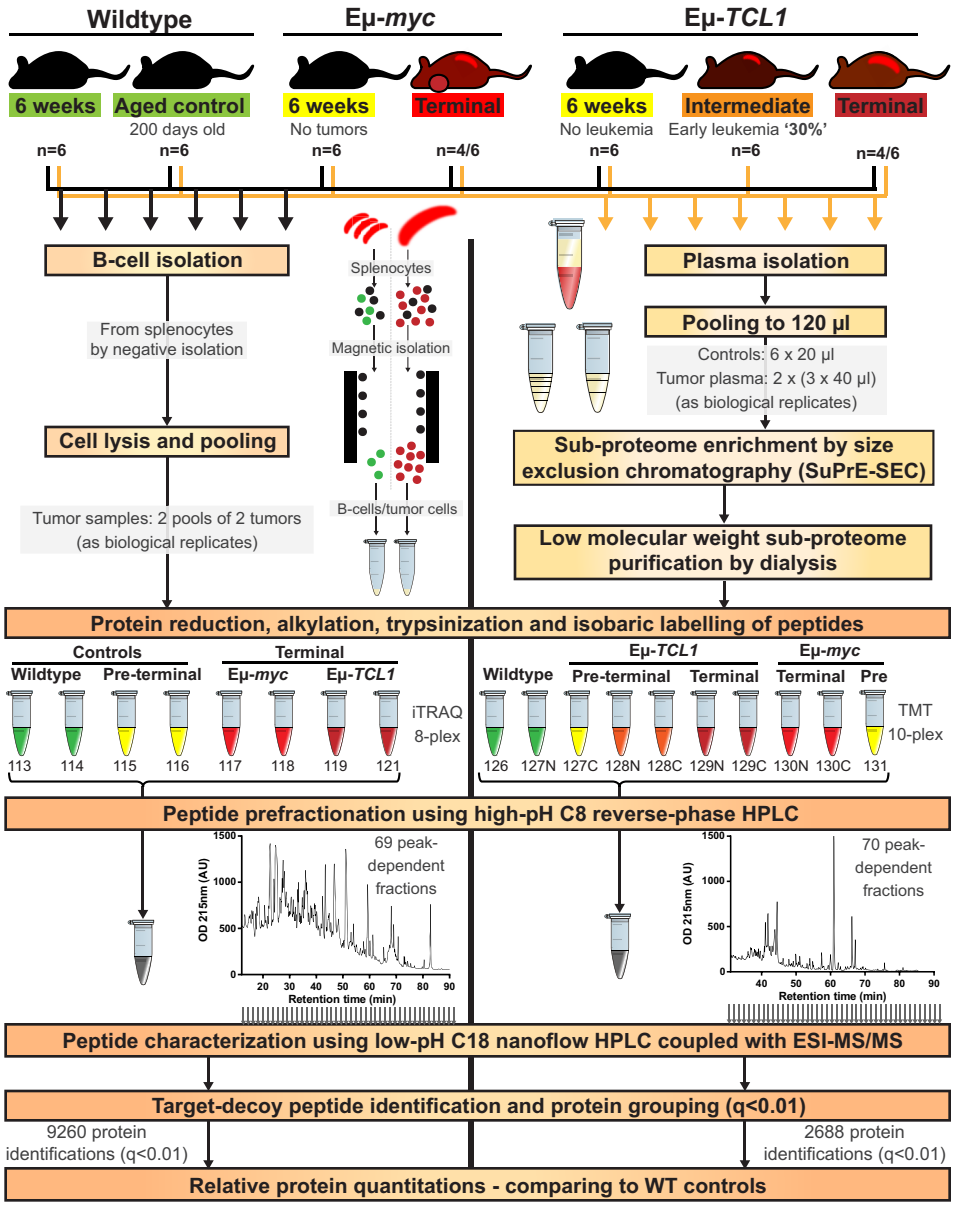

FIG. 1. **Eμ-*myc* and Eμ-*TCL1* model proteomic characterization workflow.** B-cells and plasma were isolated from splenocytes and blood, respectively, derived from terminal and preterminal Eμ-*myc* and Eμ-*TCL1* mice and WT controls (supplemental Fig. S1C). Pooling was used to accommodate all samples within single isobaric-labelled experiments for B-cell (iTRAQ 8-plex) and plasma (TMT 10-plex) proteomics. Pools of 2, 3, or 6 samples were used for tumors, tumor plasma and pretumor controls, respectively. For all tumor samples, biological replicate pools were analysed. Plasma pools, totalling 120 µl per pool, were subjected to size exclusion chromatography (SEC) to isolate the low molecular weight subproteome (supplemental Fig. S1G). B-cells were isolated by negative selection and were lysed, quantified and 100 µg of protein pooled. Plasma and B-cell proteins were subjected to reducing conditions, cysteine alkylation, trypsin proteolysis and isobaric labelling and pooling of the generated peptides. The labeled peptides for each proteome were resolved by two-dimensional liquid chromatography and quantitatively characterized by mass spectrometry (MS). The MS data were then subject to target-decoy analysis and reporter ion quantitation to generate two quantitative proteomes.

teomics correctly identified over or underexpression for the vast majority of the 38 DEPs observed by antibody-based quantitations. This comparison also highlighted reporter ion ratio compression, a commonly reported feature of isobaric tag quantitation (39, 40). Anticipated plasma proteins, such as IgM overabundance in Eμ-*TCL1* tumors, was also observed (supplemental Fig. S2I). These results therefore supported the overall reliability of the DEP observations and the characterization and analysis by which they were generated.

Proteomic Characterization of B-cell Tumor Phenotypes—Proteins were considered DEPs when both tumor pools demonstrated a clear, consistent over- or underexpression to both 6-week and 200-day WT samples. Rather than an average of the four derived ratios for each tumor, potentially misrepre-

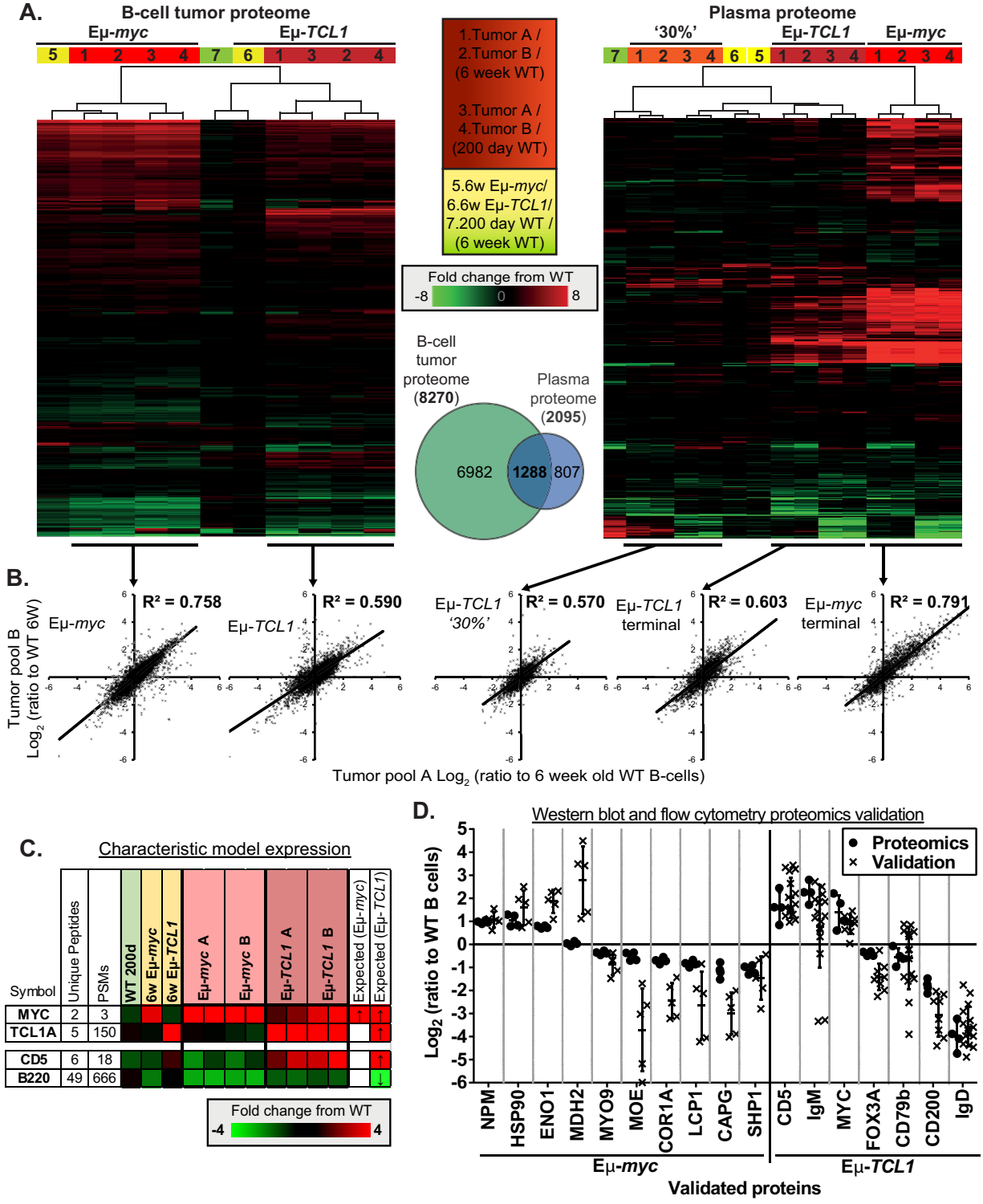

FIG. 2. **Analysis and validation of the quality of quantitative proteomics data.** *A*, Hierarchical clustering of all 8270 and 2095 fully profiled protein $\log_2$ (ratios) relative to the 6 week WT control (in addition to the 200 day WT control for tumor samples) using Cluster 3.0 and Euclidian distance to represent the topological similarities and differences for each sample. A Venn diagram highlights proteins identified in both proteomes. *B*, Linear regression highlighting the reproducibility of the $\log_2$ (ratios) relative to WT 6 week samples of the biological replicates analysed for each tumorous condition. *C*, Relative quantitative proteomics-derived fold changes of transgene-derived protein expression and characteristic Eμ-*TCL1* phenotypes, relative to WT B-cells. *D*, A summary of 17 Western blot and flow cytometry validations of Eμ-*myc* and Eμ-*TCL1* tumor protein expressions relative to WT B-cell controls, plotted alongside the proteomics-derived expression changes (as $\log_2$ (ratios)). These values relate to the validations detailed in supplemental Fig. S2*G*, S2*H*.

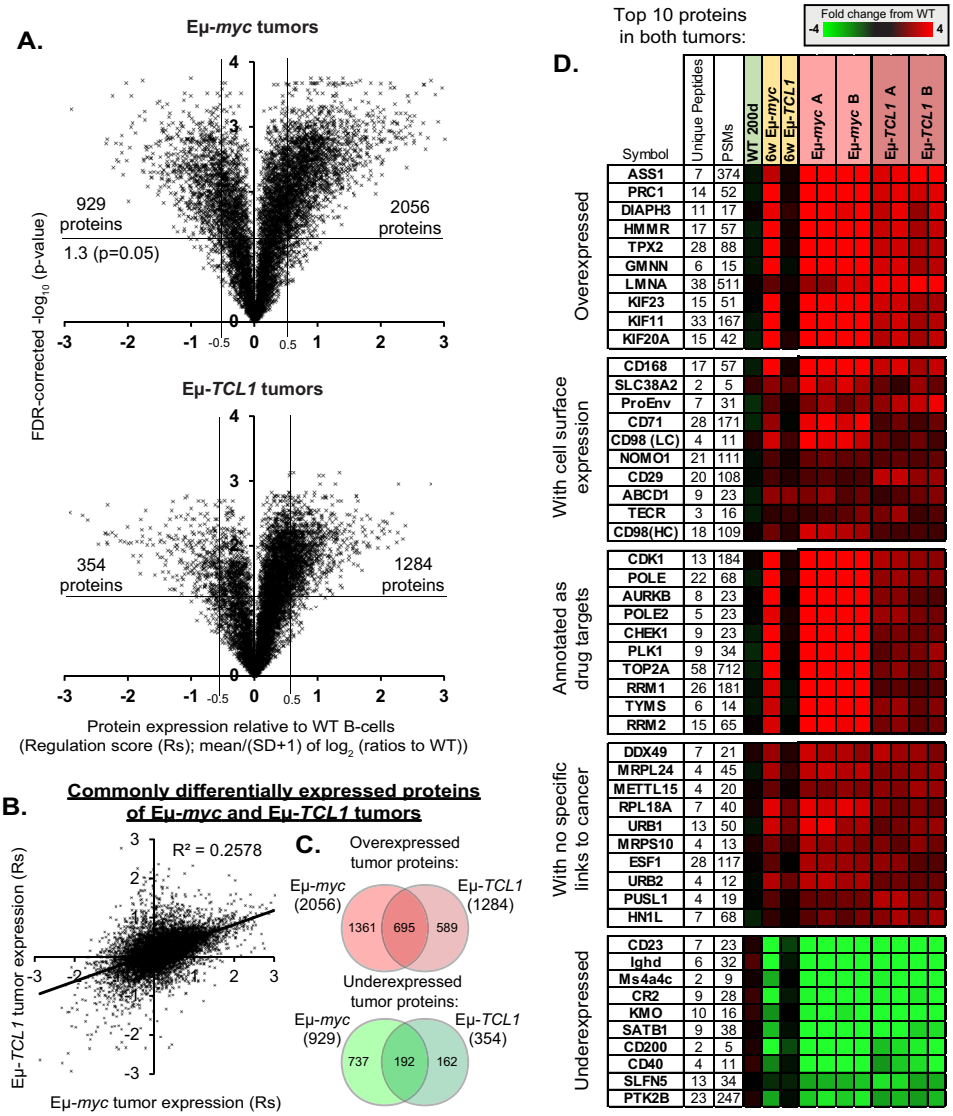

FIG. 3. **Differential protein expression in Eμ-*myc* and Eμ-*TCL1* B-cell tumors.** *A*, Volcano plots highlighting reproducible, significant differential protein expression in each B-cell tumor on the basis of the regulation score (Rs) and FDR-corrected p-values (one sample t-test). The Rs was calculated from the mean and standard deviation (SD) of the 4 $\log_2$ (ratios) of tumor protein expression relative to both WT controls (Rs = mean/(SD+1)). The number of proteins considered significantly ($p < 0.05$) overexpressed (Rs > 0.5) or underexpressed (Rs < -0.5) is detailed. *B*, A linear regression between the protein expression observed in Eμ-*myc* and Eμ-*TCL1* B-cell tumors, both relative to WT B-cells. *C*, Venn diagrams highlighting proteins considered over- and underexpressed common to both Eμ-*myc* and Eμ-*TCL1* B-cell tumors. *D*, Heat maps of individual $\log_2$ (ratios to WT), for examples of proteins differentially expressed commonly in both tumors. The top 10 proteins falling into the following categories are presented; significantly overexpressed in both tumors with high confidence (3 unique peptides and unique quantitations), cell surface expression, proteins annotated by ingenuity pathway analysis as drug targets, proteins for which no specific links to any type of cancer have previously been made, based on PubMed searching and proteins significantly underexpressed in both tumors.

sentative of variable findings, a ratio of average to standard deviation (mean/(S.D.+1)) was calculated, termed the regulation score (Rs). This provided a single value expressive of both magnitude and consistency for either, or both, tumors relative to WT B-cells. In combination with FDR-corrected *p* values, the Rs allowed careful selection of the most confidently and consistently DEPs (detailed in Supplementary Methods).

The range of significantly DEPs for each tumor were represented by volcano plot, comparing Rs to -$\log_{10}$ (*p* values) (Fig. 3*A*, supplemental Fig. S3*A*). This analysis illustrated the broad extent of DEP signatures observed in each tumor, with ~3000 and 1500 DEPs in Eμ-*myc* and Eμ-*TCL1* tumors, respectively. The 6-week Eμ-*myc* and Eμ-*TCL1* B-cells exhibited signatures broadly indistinguishable from terminal Eμ-*myc* tumors and WT B-cells, respectively (supplemental Fig. S3*B*). The 6-week Eμ-*myc* B-cell signature did however, present a lesser extent of differential expression. When compared with one another, a common signature became apparent between Eμ-

myc and Eμ-*TCL1* tumors (Fig. 3*B*) demonstrating that many of the Eμ-*myc* tumor-overexpressed proteins were also overexpressed in Eμ-*TCL1* tumors, but to a lesser magnitude. Approximately 700 and 200 proteins were considered over- and underexpressed in the tumors of both models, respectively (Fig. 3*C*). Examples of the 10 most consistently DEPs from this common signature were presented (Fig. 3*D*); and annotated as predicted cell surface markers with potential as immunotherapy targets; drug targets, annotated by IPA; and novel DEPs with no previous published links with cancer (detailed further in supplemental Fig. S3*C*–S3*G*). Among the DEPs common to both tumors were, for instance signatures of cell cycle upregulation, such as the three kinesin proteins, KIF11, KIF20A, and KIF23 and an overall trend of cell surface protein underexpression such as CD23, CR2, CD200, CD40, IgG receptor FCGRT, CD38, CD22, and IL21R. The most consistently overexpressed surface proteins, HMMR/CD168, has previously been associated with B-cell cancers (41, 42).

Bioinformatics Reveals Signatures Common to Contrasting B-cell Tumors—Although individual DEPs can suggest functional insight, approaches simultaneously considering all DEPs, potentially offer a broader understanding of biological mechanisms. Accordingly, topological, proteome-wide expression patterns were investigated by bioinformatics.

Gene ontology (GO) term enrichment was used to identify processes overrepresented by the DEPs observed in both tumors (Fig. 4*A*, supplemental Table S3). Among the overexpressed proteins GO term enrichment identified strong signatures of mechanisms relating to cell growth and proliferation, including; "ribosome biogenesis" ($n = 106$, $p = 1.8 \times 10^{-27}$), "translation" ($n = 135$, $p = 1.2 \times 10^{-16}$), "chromosome segregation" ($n = 81$, $p = 6.0 \times 10^{-14}$) and "cell cycle" ($n = 229$, $p = 2.5 \times 10^{-11}$). Among the underexpressed proteins were trends of several immune function-related terms, such as lymphocyte activation ($n = 41$, $p = 8.8 \times 10^{-7}$), Ig-mediated immune response ($n = 15$, $p = 2.1 \times 10^{-5}$), and BCR signaling ($n = 11$, $p = 2.9 \times 10^{-4}$). Additionally, several processes related to immune evasion, differentiation, and growth inhibition were enriched.

To visualize these processes and highlight the proteins contributing to the enriched GO terms, networks were displayed descriptive of individual proteins and their interrelationships, defined by STRING (43). Fig. 4*B* demonstrates a network generated from proteins annotated with "chromosome segregation" highlighting the scale and complexity of the dysregulation of this process seen in both tumors. "Ribosome biogenesis" was also illustrated in this way (Fig. 4*C*), highlighting those overexpressed proteins responsible for the term's enrichment. A cluster of interacting ribosome proteins was identified, alongside several assembly regulators. Several canonical pathways, including ribosome-, translation-, and cell cycle-related pathways demonstrated significant enrichment in both tumors (supplemental Fig. S4*A*). A network detailing all underexpressed proteins revealed a highly interrelated series of interactions highlighting major histocompatibility complex proteins, interferon response proteins and B-cell-related signaling molecules (Fig. 4*D*).

To simultaneously analyze both proteome-wide over- and underexpression, upstream regulators were evaluated using IPA. Upstream regulator activity was inferred by the comparison of anticipated downstream expression profiles of proteins with those expression profiles derived by quantitative proteomics for both tumors (supplemental Table S3, supplemental Fig. S4*B*–S4*E*). Protein functionality was then inferred from a combination of the resulting upstream regulator activation z-scores—a value proportional to overall predicted activation (44)—and the proteomics-determined differential expression (Fig. 4*E*). Several regulators not quantitated by proteomics, including miRNA were also inferred to be activated or inactivated (supplemental Fig. S4*C*, S4*E*).

Myc overexpression and inferred activation (Rs = 1.11, z = 8.09, $p = 6.6 \times 10^{-26}$), alongside other proliferative drivers and oncogenes (*e.g.* E2F3, MYCN, RABL6 (Rs>0.5, z>4)) described several key, functional regulators influencing the neoplastic B-cell phenotype (Fig. 4*E*, supplemental Table S3). The combined overexpression and inferred inactivation of TP53 (Rs = 0.97, z = −3.76, $p = 1.6 \times 10^{-34}$) and retinoblastoma 1 (RB1) (Rs = 0.59, z = −2.86, $p = 2.3 \times 10^{-21}$), represented an anticipated evasion of tumor suppressor pathways. Interestingly, RB1-like 1 (RBL1) (Rs = 0.92, z = −4.47, $p = 2.2 \times 10^{-16}$), a lesser-established tumor suppressor, had greater overexpression and inferred inhibition than its better-studied family member.

It was additionally possible to compare differential protein phosphorylation to infer activation or inhibition (supplemental Fig. S4*F*–S4*H*). HDAC2 overexpression in Eμ-*myc* tumors, for instance, was accompanied by a signature of downstream inactivation (supplemental Fig. S4*B*) and a decreased phosphorylation of Ser^{394} (supplemental Fig. S4*H*), a modification previously associated with the activation of HDAC2 (45). Similarly, in Eμ-*TCL1* tumors, RBL1 overexpression was accompanied by apparent inactivation and decreased Thr^{385} phosphorylation. Differential phosphorylation of BCR signaling pathway components demonstrated an increased phosphorylation of downstream proteins such as NF-κB, OCT2 and ETS1 (supplemental Fig. S4*J*).

Characteristics Specific to Eμ-myc B-cell Tumors—Although the common tumor signature in both models was strong, several tumor-specific differences were also apparent, particularly in the more aggressive Eμ-*myc* tumors. To evaluate tumor-specific expression, proteins were filtered to include those which exhibited significant over- or underexpression in one tumor model (Rs>0.5/<-0.5, $p < 0.05$) but not the other (Rs>0.25/>-0.25). This identified 572 and 537 proteins with specific over- or underexpression in Eμ-*myc* tumors, respectively. The 10 most over- and underexpressed proteins

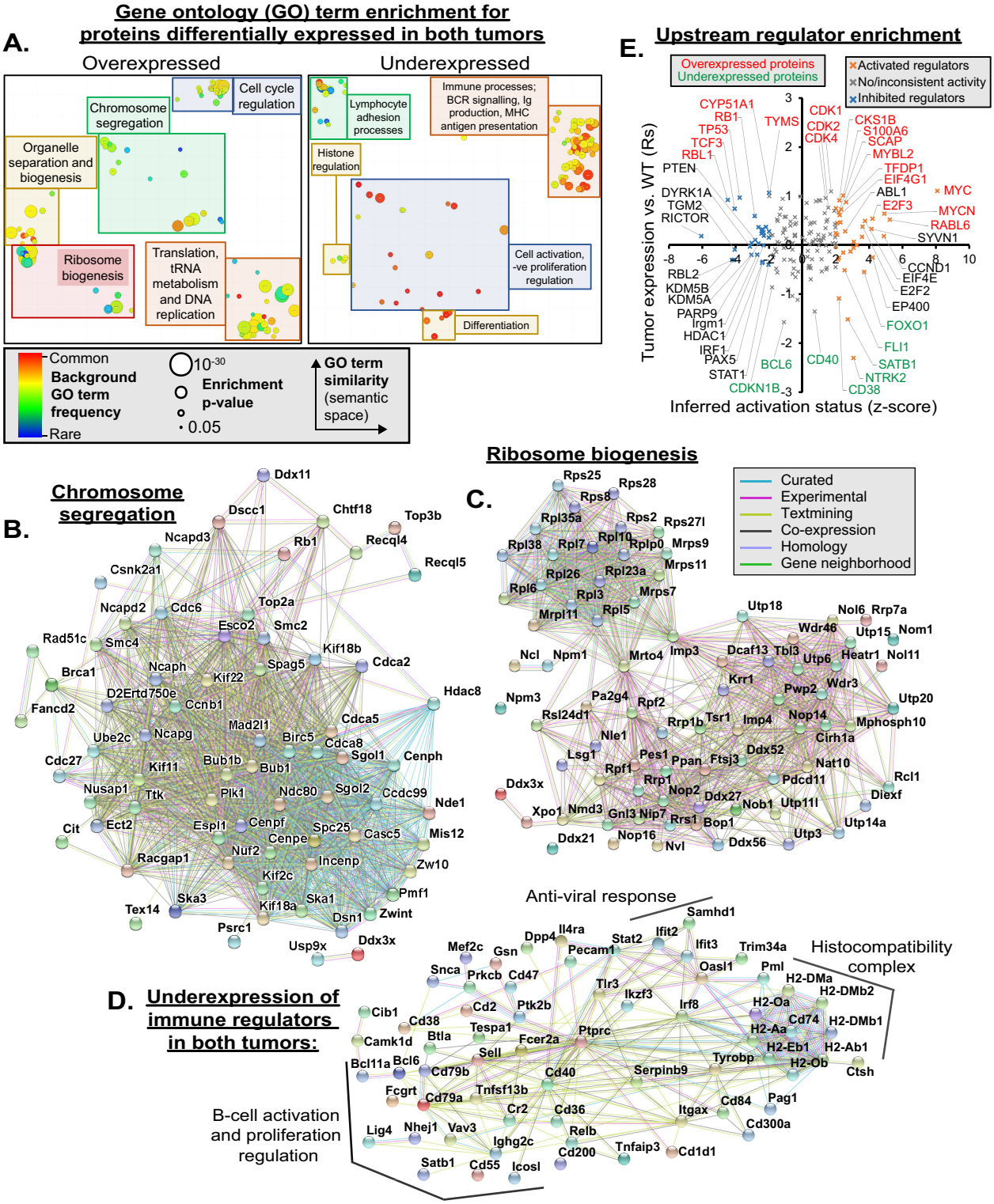

FIG. 4. **Bioinformatic interrogation of commonly differentially expressed B-cell tumor proteins.** *A*, Gene ontology (GO) term enrichment analysis for proteins over- and underexpressed in both tumors, visualized using Revigo (94) and summarized based on parent GO terms and Revigo-defined semantic space. *B–D*, StringDB networks highlighting interactions and relationships for proteins; *B*, overexpressed in both tumors annotated with the term 'chromosome segregation' (GO:0007059) (n = 81), *C*, overexpressed in both tumors annotated as "ribosome biogenesis" (GO:0042254) (n = 106), and *D*, those proteins underexpressed in both tumors relating to terms descriptive of immune regulation. *E*, Upstream regulator activation z-scores inferred by IPA for all consistently differentially expressed B-cell tumor proteins, plotted against tumor protein expression, relative to WT B-cells. A positive z-score indicates a signature of protein activation.

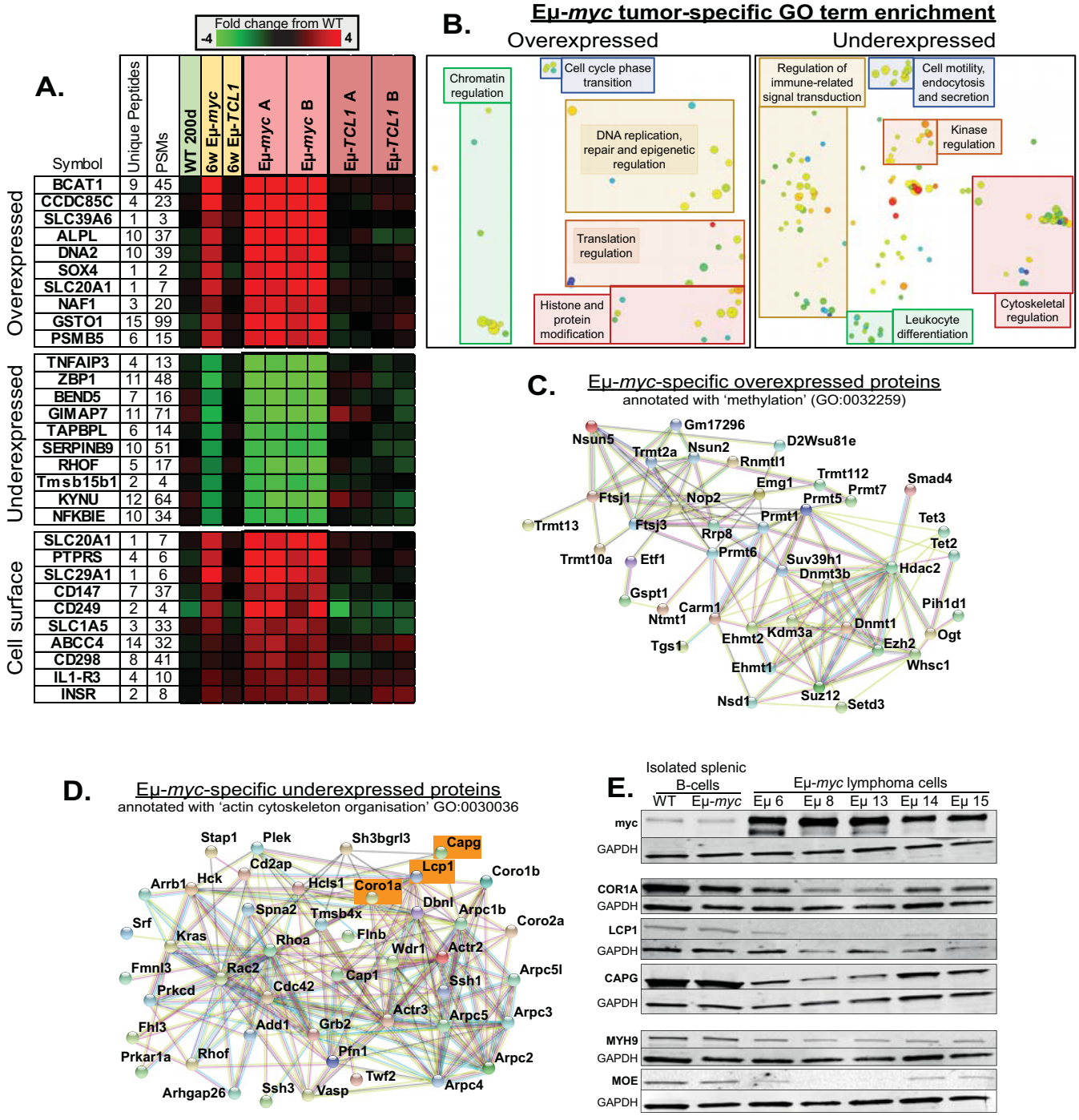

FIG. 5. **Eμ-*myc*-specific tumor characteristics.** *A*, Heat maps of individual $\log_2$ (ratios to WT), for the top 10 proteins specifically over- and underexpressed in Eμ-*myc* tumors (Rs $_{E\mu\text{-}myc}$ >0.5/<-0.5, p <0.05, Rs $_{E\mu\text{-}TCL1}$ <0.25/>-0.25). Additionally, the top 10 proteins with specific cell surface expression are shown. *B*, GO term enrichment analysis for differential expression specific to Eμ-*myc* tumors (as described for Fig. 4). *C–D*, StringDB networks derived from Eμ-*myc*-specific differentially expressed proteins annotated with *C*, "methylation" (GO:0032259) (n = 50), and *D*, "actin cytoskeleton organization" (GO:0030036) (n = 49). *E*, Western blot evaluation of the three "actin cytoskeleton organization"-annotated proteins, coronin 1a (COR1A), lymphocyte cytosolic protein 1 (LCP1) and actin regulatory protein CAPG, expression in Eμ-*myc* tumors, relative to nontumor B-cells. Two addition cytoskeletal proteins, myosin-9 (MYH9) and moesin (MOE) are also evaluated alongside myc.

in addition to cell surface proteins were illustrated to highlight examples of this specific differential expression pattern in Eμ-*myc* tumors (Fig. 5*A*).

The over- and underexpressed proteins specific to Eμ-*myc* tumors were evaluated, as for Fig. 4*A*, for GO term enrichment (Fig. 5*B*, supplemental Fig. S3). The majority of GO terms

observed for both tumors were also observed for the Eμ-*myc*-specific proteins, further highlighting trends of increased proliferation and growth of cells. Exceptions included trends of epigenetic-related processes and underexpressed cytoskeletal processes.

Most notably specific to overexpressed Eμ-*myc* tumor proteins was the enrichment of the term "methylation" ($n = 50$, $p = 0.03$). A network was formed from these 50 proteins (Fig. 5*C*), highlighting overexpressed methylation enzymes relating to gene expression; both epigenetically (histone methylation, $n = 18$) and post-transcriptionally (RNA methylation, $n = 10$). CpG methylation appeared widely dysregulated with 2/3 methylation (DNMT1, DNMT3B) and 2/3 demethylation (TET2, TET3) enzymes overexpressed.

Eμ-*myc* tumors demonstrated a broad downregulation of processes relating to the cytoskeleton, for example, "actin cytoskeleton organization" ($n = 49$, $p = 1.2 \times 10^{-6}$), as illustrated in a network (Fig. 5*D*). This illustrated the underexpression of six actin-related protein 2/3 complex subunits (ARPC) and three coronin proteins. Three interrelated proteins from this network, coronin 1a (COR1A), lymphocyte cytosolic protein 1 (LCP1) and actin regulatory protein CAPG, were evaluated for relative expression in Eμ-*myc* tumors, relative to nontumor B-cells by Western blot (Fig. 5*E*). In each instance, underexpression was observed in line with that of the quantitative proteomics findings (compared in Fig. 2*D*). Additionally, myc overexpression was evaluated alongside two further cytoskeleton-related proteins; a broadly functioning regulator of cytoskeletal activity, myosin-9 (MYH9) and a cytoskeletal-membrane junction protein, moesin (MOE) again demonstrating anticipated differential expression.

Characteristics Specific to Eμ-TCL1 B-cell Tumors—Protein expression specific to Eμ-*TCL1* tumors was also evaluated, with the top 10 DEPs and membrane proteins presented (Fig. 6*A*). As validation this illustrated the discrete expression of human TCL1 (supplemental Fig. S2*A*) in Eμ-*TCL1*-derived B-cell samples. GO term enrichment identified upregulated processes relating to intracellular compartments, such as ER stress, vesicular transport and glycosylation. Extracellular interactions, including signaling, locomotion and adhesion appeared as the strongest underexpressed process in Eμ-*TCL1* tumors (Fig. 6*B*). A network formed from Eμ-*TCL1*-specific overexpressed proteins (Fig. 6*C*) presented clusters of associated proteins contributing to enriched GO terms, such as ER and golgi proteins. Several signaling proteins were also specifically overexpressed, such as phosphatidylinositol kinases and phosphatases. Associated with these signaling proteins were the alpha and beta subunits of the interleukin 5 receptor (IL5Rα and IL5Rβ), also apparent among the top 10 membrane proteins, highlighted in Fig. 6*A*.

Interleukin 5 Receptor is Overexpressed by Eμ-TCL1 B-cell Tumors—The overexpression of the IL5R was first evaluated by plotting the individual iTRAQ ratios for each unique peptide matching IL5Rα and IL5Rβ (Fig. 6*D*, supplemental Fig. S5*A*–S5*E*). For both IL5R subunits a clear, specific overexpression was apparent. Furthermore, the signature for IL5 activity was apparent through various bioinformatics analyses, including IPA regulator analyses (supplemental Fig. S4*C*, S5*F*). A signature additionally became apparent in Eμ-*TCL1* terminal and preterminal plasma indicative of an IL5-induced proliferation signature, as well as plasma signatures of quantitated proteins and inferred regulators potentially upstream of IL5 induction (supplemental Fig. S5*G*–S5*I*).

Given the strength of this evidence, the surface expression of IL5Rα, the subunit specific to IL5 recognition, was evaluated by flow cytometry for terminal and pretumor Eμ-*TCL1* B-cells, relative to WT B-cells (Fig. 6*E*, supplemental S5*J*–S5*K*). Although IL5Rα expression was observed across a wide distribution for WT B-cells, for pretumor Eμ-*TCL1* B-cells, the emerging $CD5^+$ population was observed with high IL5Rα expression. The Eμ-*TCL1* tumor cells exhibited the same $CD5^+IL5R\alpha^+$ expression as the emerging pretumor Eμ-*TCL1* B-cell population.

Interleukin 5 Drives Proliferation in Eμ-TCL1 B-cell Tumors via AKT—The observation of substantial overexpression of both IL5Rα and IL5Rβ, strongly suggested a functional role for the IL5R and IL5 in driving Eμ-*TCL1* tumors. To investigate and functionally validate the IL5R overexpression, terminal tumors from Eμ-*TCL1* mice were treated with 0, 10 and 100 ng/ml of IL5 for 48 h *in vitro*. First, cell density indicated a dose-dependent expansion induced by IL5 (Fig. 7*A*). CFSE labeling confirmed that cells were proliferating in a dose-dependent manner with as many as 70% of cells being postmitotic after 48 h of 100 ng/ml IL5 treatment (Fig. 7*B*). Furthermore, evaluation of cell cycle phases by hypotonic PI staining demonstrated that almost three times as many cells (14.5%) were in $S/G_2/M$ phase after 100 ng/ml IL5 treatment, compared with no treatment (4.9%) (Fig. 7*C*).

Given the proposed role of TCL1 in amplifying AKT signaling (16, 17), AKT activation by IL5 was investigated (Fig. 7*D*). Serum starvation and the subsequent addition of IL5 induced AKT phosphorylation in a dose-dependent manner at doses of greater than 5 ng/ml. Downstream signaling (summarized in Fig. 7*E*) was also apparent, with dose-dependent phosphorylation of the S6 ribosomal protein and S6 kinase, indicative of mTOR activation.

Plasma proteomics reveals signatures of tumor lysis and immune response—To investigate the overall plasma proteome signature, those proteins quantified commonly or discretely within the B-cell and plasma proteomes (supplemental Table S2) were dissected based on canonical protein localizations (Fig. 8*A*). The vast majority (82%) of the 1288 proteins observed as common to both proteomes, were annotated with a canonical cellular localization, compared with just 40% of proteins identified discretely in the plasma proteome. Furthermore, evaluation of the relative abundances in terminal tumor plasma revealed a striking signature of overabundant cell-derived proteins (Fig. 8*B*). The tumor origin of this plasma

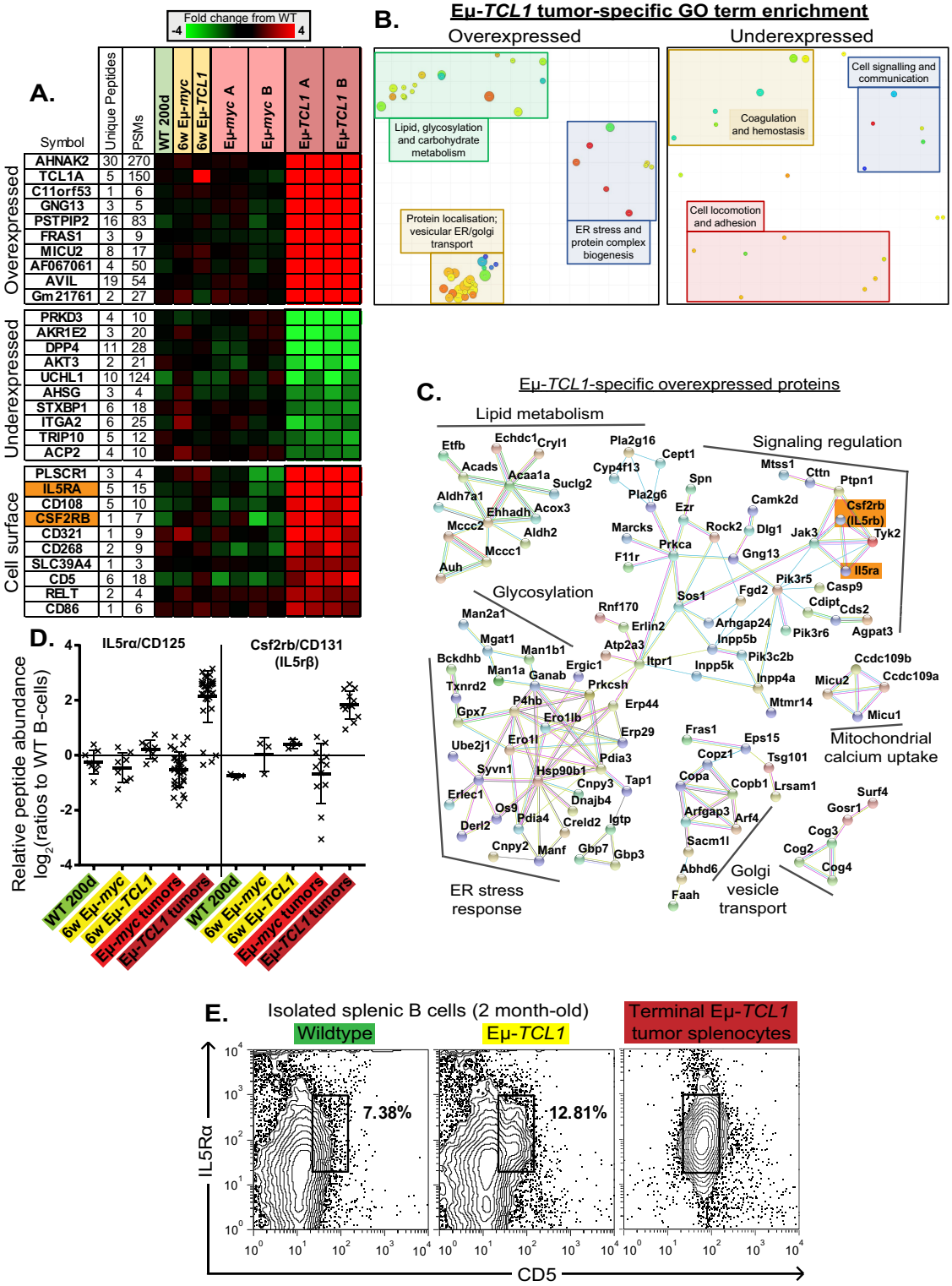

FIG. 6. **Eμ-*TCL1*-specific tumor characteristics.** *A*, Heat maps for proteins and surface proteins specific to Eμ-*TCL1* tumors (Rs $_{E\mu\text{-TCL1}}$ >0.5/<-0.5, p<0.05, Rs $_{E\mu\text{-myc}}$ <0.25/>-0.25). *B*, GO term enrichment analysis for differential expression specific to Eμ-*TCL1* tumors. *C*, A StringDB network derived from Eμ-*TCL1*-specific differentially expressed proteins demonstrating interaction scores of >0.7 highlighting processes in protein clusters. (ER; endoplasmic reticulum). *D*, Individual iTRAQ quantifications (as $\log_2$ (ratios to WT)) for the peptides uniquely matching to IL5RA and it receptor partner CSF2RB (IL5RB). *E*, Flow cytometry evaluation of IL5 receptor alpha subunit (IL5Rα) expression on an Eμ-*TCL1* tumor (representative of four evaluated tumors (supplemental Fig. S5*K*)), compared to splenic B cells pooled and isolated from three 2-month-old WT and Eμ-*TCL1* mice.

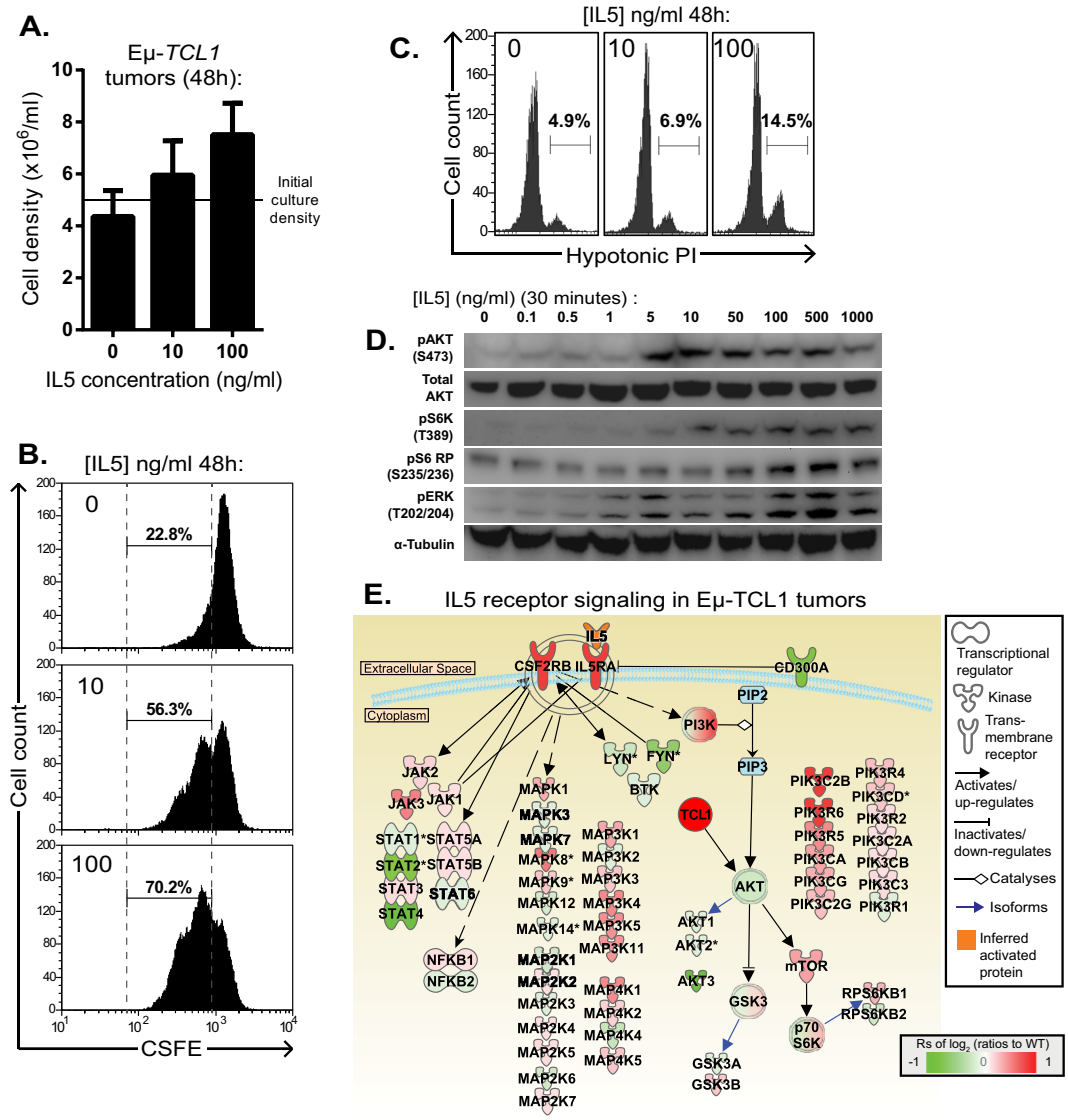

FIG. 7. **IL5 drives Eμ-*TCL1* tumor proliferation.** *A*, Tumor cells from three spleens of terminal Eμ-*TCL1* mice were cultured at an initial density of 5×10^6 cells/ml and treated in with IL5. Cell density was measured after 48 h, and the mean and SD presented. *B*, Cell division analysis measured by CFSE staining of terminal Eμ-*TCL1* tumors treated *in vitro* with 0, 10, or 100 ng/ml IL5 for 48 hours *C*, IL5-treated Eμ-*TCL1* tumors (48 h) were stained with hypotonic propidium iodide and DNA content measured with flow cytometry to determine the proportion of cells entering mitosis. *D*, Serum starved (4 h) Eμ-*TCL1* tumor cells were evaluated for IL5 treatment dose response after 30 minutes by Western blotting for the phosphorylation of AKT, ERK, S6, and S6K. *E*, Summary of potential signal transduction pathway components, overlaid with Eμ-*TCL1* tumor proteomics quantitations, highlighting a mechanism of IL5-induced AKT phosphorylation, amplified by TCL1.

signature was additionally indicated by GO term enrichment (Fig. 8*C*), with highly similar trends to that of the B-cell tumors (Fig. 4*A*), and an inter-proteome correlation between the approximate protein abundances (supplemental Fig. S6*A*). Additionally proteins were illustrated with biomarker applications (supplemental Fig. S6*H*), specific tumor plasma signatures (supplemental Fig. S6*J*–S6*P*), differential abundance relative to approximate relative plasma concentrations (supplemental Fig. S6*Q*), over- and underabundance in both the tumor and plasma proteomes (supplemental Fig. S6*R*) and with potential as biomarkers derived from functional tumor regulators (supplemental Fig. S6*S*–S6*T*).

To explore differential protein abundance resulting from the extrinsic response to the tumor, the plasma proteome was subject to deconvolution, removing proteins with a clear cellular origin. The remaining proteins, termed the "lysis-free" plasma proteome (supplemental Table S2, supplemental Fig. S6*F*), provided a signature descriptive of an immune response. Terms including "defense response" ($n = 16$, $p = 4.0 \times 10^{-5}$) and "extrinsic apoptotic signaling

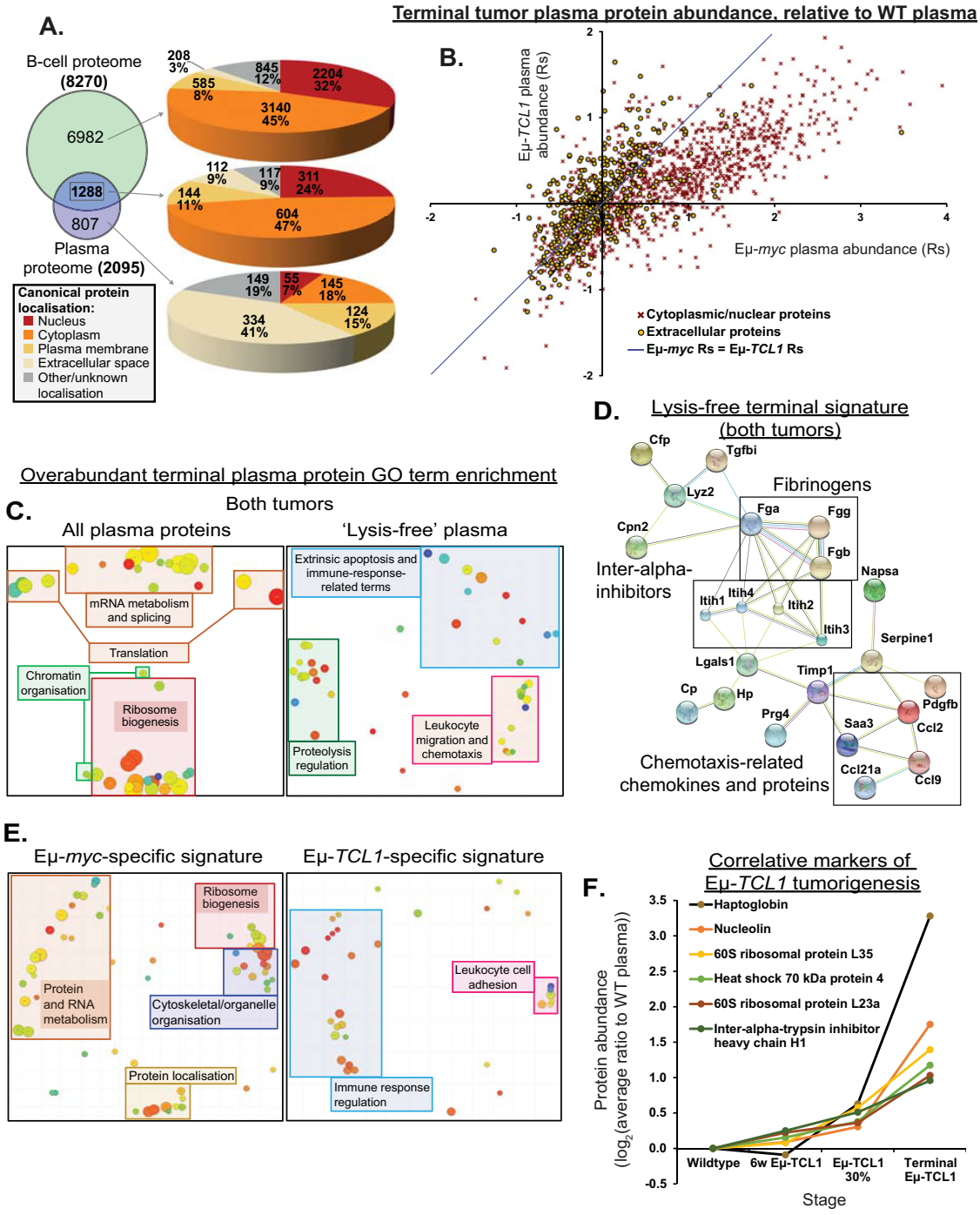

FIG. 8. **Model-dominant plasma signatures of Eμ-*myc* and Eμ-*TCL1* tumors.** *A*, Interproteome comparison detailing the canonical cellular localizations, annotated by Ingenuity Pathway Analysis (IPA), of proteins commonly or discretely quantified in plasma or B-cells. *B*, The relative plasma protein abundances relative to WT plasma for terminal Eμ-*myc* and Eμ-*TCL1* tumors, highlighting those proteins annotated as intracellular (cytosolic/nuclear proteins) and extracellular. *C*, GO term enrichment for plasma proteins overabundant in both tumors, considering all plasma proteins and additional analyzing only those extracellular proteins not traceable to the B-cell tumor proteome, termed the "lysis-free" plasma. D. StringDB networks highlighting interactions and relationships for proteins overabundant in the "lysis-free" plasma for both tumors. *E*, GO term enrichment for plasma proteins overabundant specific to each tumor (Rs $>$ 0.5 and $p < 0.05$, $Rs_{other\ tumor}<0.5$). *F*, Proteins demonstrating progressive increases in abundance correlating with tumorigenesis in Eμ-*TCL1* mice.

pathway via death domain receptors" ($n = 6$, $p = 1.4 \times 10^{-4}$) were identified as enriched among these overabundant "lysis-free" plasma proteins (Fig. 8*C*). To detail this lysis-free signature further, a network was generated from all overabundant lysis-free plasma proteins (Fig. 8*D*). Protein clusters included chemotaxis regulators Ccl2, Ccl9 and

Ccl21a, wound and inflammation response proteins, fibrinogens α, β, and γ and the hyaluronan-binding, interalpha-trypsin inhibitor proteins, ITIH1-ITIH4.

Comparison between the terminal plasma signatures for each tumor model (Fig. 8*B*) demonstrated the dominance of this tumor lysis signature in Eμ-*myc* tumors, whereas Eμ-*TCL1* terminal plasma contained a dominant signature of extracellular proteins. In both cases these signatures were observed for the opposing tumor, but to a lesser extent. GO term enrichment for overabundant plasma proteins specific to Eμ-*myc* and Eμ-*TCL1* terminal tumors illustrated model-specific signatures of tumor lysis and extracellular proteins, respectively (Fig. 8*E*). Eμ-*myc* tumor plasma specific GO terms had a strong resemblance to that of the B-cell tumors, highlighting cellular processes similar to both the tumors and the common plasma signature (Fig. 4*A* and 8*C*). Overabundant plasma proteins specific to terminal Eμ-*TCL1* tumors enriched for several GO terms related to immune processes, such as "immune response" ($n = 17$, $p = 1.5 \times 10^{-4}$) and "lymphocyte activation" ($n = 12$, $p = 4.8 \times 10^{-4}$).

Finally, consideration was given to proteins emerging in the preterminal "30%" Eμ-*TCL1* plasma (Fig. 8*F*). Plasma proteins demonstrating a correlation between overabundance and tumorigenesis were plotted, highlighting the extracellular immune-response proteins haptoglobin (Hp) and ITIH1, both also observed in the lysis free signature. Several additional proteins demonstrating overabundance in preterminal "30%" Eμ-*TCL1* plasma are detailed in supplemental Fig. S6*I*.

DISCUSSION

B-cell tumors have been intensively investigated by genomics and transcriptomics in recent years, advancing clinical and biological understanding (46–49). Such information, is however sometimes limited, especially in a functional context, because of the weak correlations observed between mRNA and protein expression (50, 51). A comparison between our proteomics data and a former Eμ-*myc* tumor mRNA expression data set (supplemental Fig. S2*J*) highlighted an example of this, demonstrating an anticipated but limited correlation (52). Furthermore, genomics and transcriptomics are limited in capturing organism-wide tumor biology from acellular samples such as plasma.

This study aimed to combine and implement recent advances in quantitative MS proteomics to comprehensively characterize the tumors and plasma of contrasting mouse B-cell cancer models; Eμ-*myc* and Eμ-*TCL1*. By comparing tumors driven by contrasting oncogenes, with differing phenotypes and rates of progression, any apparent common signatures could suggest the most conserved and essential B-cell cancer mechanisms. Model-specific signatures could provide insight into the molecular basis of the discrete cancer phenotypes and oncogenes, potentially of relevance to BL and CLL. Simultaneous plasma characterization offered potential insight into tumor-host dialogue, systemic cancer impacts and biology of biomarker emergence. Furthermore, greater understanding of these models offers an opportunity to appreciate their strengths and weaknesses in preclinical applications.

Overall, isobaric-labeled LC-MS proteomics of B-cell and plasma samples (Fig. 1) provided biologically reproducible (Fig. 2*A*, 2*B*), high-depth (supplemental Fig. S1*H*) and representative (supplemental Fig. S1) characterizations of the Eμ-*myc* and Eμ-*TCL1* tumor models. The accuracy of the quantitative results was validated by anticipated transgene expression (Fig. 2*C*), Western blotting and flow cytometry (Figs. 2*D*, supplemental Fig. S2*G*, S2*H*) alongside comparisons to previously published protein expressions (supplemental Fig. S2*D*, S2*F*) and mRNA expression data (supplemental Fig. S2*J*). Interestingly, a brief analysis revealed that those proteins overexpressed without corresponding mRNA overexpression were enriched with proteins annotated with the term "translation."

A Common B-cell Tumor Signature in Divergent Models—The expression correlation between the contrasting Eμ-*myc* and Eμ-*TCL1* tumors (Fig. 3*B*) was indicative of a common B-cell tumor signature that was proportional to aggression. Indeed, this signature strongly highlighted canonical tumor characteristics such as upregulated cell proliferation and growth (Fig. 4). Furthermore, frequent observations of these overexpressed proteins in several human cancers (supplemental Fig. S3*C*) highlighted potential relevance to non-B-cell cancers. This was particularly noteworthy, given the many clinically relevant cell surface proteins and drug targets characterized (Fig. 3*D*, supplemental S3*F*, S3*G*). HMMR/CD168, for instance, has previously been considered as an immunotherapy target in B-cell cancers (41, 53). Similarly, amino acid and zinc transporter overexpression could offer targets of metabolic inhibition or immunotherapy. The observation of proteins, and even putative proteins, in this common B-cell tumor signature with no prior links to cancer offers several new hypotheses (supplemental Fig. S3*E*). DDX49 and MAK16, for instance, are poorly characterized proteins overexpressed in all four tumor pools, and could be inferred to have a role in ribosome biogenesis, given their homology, orthologous functions and the prevalence of ribosome biogenesis upregulation in both tumors.

Downregulation of immune functions were indicative of the loss of B-cell characteristics, not essential and potentially even inhibitory toward tumor development. Constitutive Ig synthesis, for instance, would provide a negative selective pressure on resource-limited tumor cells. MHC component underexpression suggested a clear mechanism of immune evasion, described previously (54, 55).

Model Specific Signatures of Eμ-myc and Eμ-TCL1 Tumors—Eμ-*myc*- and Eμ-*TCL1*-specific DEPs (Figs. 5–6) highlighted distinct expression patterns responsible for the contrast in tumor phenotypes; such as the vast protein dysregulation and proliferation produced by the aggressive

and pleiotropic nature of myc. The contrast between these models was also apparent prior to tumorigenesis (supplemental Fig. S3*B*), with little to no tumor signature in 6-week Eμ-*TCL1* B-cells, whereas Eμ-*myc* 6-week old B-cells were almost indistinguishable from terminal tumors. Although none of these 6-week Eμ-*myc* mice presented with splenomegaly, metastases or ill health, it remains possible that tumor development was present at an early stage in one or more of the mice. Eμ-*myc*-specific DNA and histone methylation dysregulation (Figs. 5*B*, 5*C*) suggests dynamic epigenomic instability as a basis of myc-induced tumor characteristics, previously observed in B-cell lymphomas (56, 57). This potentially drives accelerated trait acquisition via nonmutational evolution (58).

Broad underexpression of actin cytoskeletal organizing components was potentially indicative of defects to normal B-cell migration and adhesion (Fig. 5*D*), identifying a possible mechanism promoting lymph node metastases; frequently observed for Eμ-*myc* tumors. These proteins may also have been underexpressed as a result of redundant immune-related functions such as those described in Fig. 4*D*. Of the three inter-connected actin cytoskeletal organizing proteins validated with underexpression (Fig. 5*E*), all three demonstrated both immune and cytoskeletal function. Cor1A promotes F-actin disassembly and cell motility (59) and mutations have been shown to impair lymphocyte function (60, 61). LCP1 regulates actin bundling and B-cell development (62, 63), whereas LCP1 knock out impaired B-cell migration (64). CAPG caps actin filaments with CAPG$^{-/-}$ mice exhibiting immune defects (65). Given observations of the pro-metastatic nature of these proteins in nonlymphocyte tumors (66, 67), this indicated metastasis may be a more passive event for Eμ-*myc* tumors. Overexpression of adhesion components such as integrin beta 1 may have facilitated this. Noncanonical cytoskeletal component AHNAK, a titin-related and cancer-associated cytoskeletal protein, shown to be essential for migration and invasion (68); was overexpressed in Eμ-*myc* tumors, potentially highlighting an alternative metastatic pathway. Additionally, other cytoskeletal components such as those directing chromosome segregation were overexpressed. Validation of two further underexpressed proteins extended the observation of cytoskeletal dysregulation, with moesin and myosin-9 annotated with roles in leukocyte migration. Together these observations suggest a trend for further investigation.

The Eμ-*TCL1*-specific features, such as ER stress response and aberrant glycosylation upregulation (Fig. 6*B*–6*C*) have previously been observed (69). Additional features, such as integrin-α2 underexpression, transmembrane protein processing, post-translational modification, transport and membrane lipid composition, may suggest several potential mechanisms by which circulatory, leukemic cell formation may be promoted in Eμ-*TCL1* tumors.

Generally unaltered BCR pathway component expression, relative to the underexpression observed for Eμ-*myc* tumors, indicates a role for antigen-receptor signaling in Eμ-*TCL1* tumors, observed previously (70) (supplemental Fig. S4*J*). This highlights potential examples of negative regulation or redundant functions for tumor growth and survival *e.g.* BCL6, FOXO1, and CD45. Upregulated phosphorylations, such as PI3Ks and FOXO1, specifically in Eμ-*TCL1* tumors may also illustrate tumor mechanisms (supplemental Fig. S4*J*, supplemental Table S4).

Interleukin 5 Receptor Overexpression and Signaling in Eμ-TCL1 Tumors—Signaling dysregulation (Fig. 6*C*) and increased expression and phosphorylation of PI3Ks (supplemental Fig. S4*J*) suggested the presence of strong receptor signaling underlying Eμ-*TCL1* tumorigenesis. IL5R overexpression (Fig. 6, supplemental Fig. S5) strongly implied a role for the IL5:IL5R signaling pathway in Eμ-*TCL1* tumors. Although not previously described in Eμ-*TCL1* mice, other mouse CLL-like B-cell tumors have demonstrated IL5 sensitivity (71–74), in addition to a CLL-like leukemia arising in mice with constitutive overexpression of IL5 (75).

The dose-dependent proliferation of Eμ-*TCL1* tumor cells upon IL5 treatment (Fig. 7*A*–7*C*) provided additional, functional validation of IL5R overexpression. IL5R signaling has been suggested to induce activation of Lyn, JAK2, Syk, BTK, NF-κB, and PI3K (76–78). Given the suggested role of AKT amplification by TCL1, PI3K signaling was a likely candidate for the effectuation of the IL5 response. Indeed, the PI3K catalytic subunit type 2 beta (PIK3C2B), alongside other PI3K isoforms, appeared as the most overexpressed of the IL5R downstream signaling molecules. Dose-dependent AKT phosphorylation upon IL5 treatment confirmed a role for the PI3K pathway, highlighting TCL1 as a potential factor in the amplification of IL5R signaling (Fig. 7*D*–7*E*).

The observation of IL5RA expression by the expanded CD5^{+} peritoneal and splenic B-cell populations in young Eμ-*TCL1* mice (supplemental Fig. S5*J*) strongly suggests a precursor cell population with characteristics of B-1 B-cells. Given the induction of B-cell proliferation observed with IL5 (79, 80) and that IL5$^{-/-}$ mice are deficient for CD5^{+} B-1 B-cells (81), IL5R signaling emerges as a probable component driving Eμ-*TCL1* tumorigenesis from CD5^{+} IL5RA^{+} B-1 B-cells.

The role for IL5 in B-cells, and B-cell tumors, appears to not be conserved between species (80, 82) highlighting a limitation in the recapitulation of human CLL with previous reports suggesting IL5 induces spontaneous apoptosis in these cells (83). However, the similarities of IL5R signaling in Eμ-*TCL1* tumors with IL4 signaling in CLL, suggest continued potential for Eμ-*TCL1* mice in modeling many aspects of the human disease.

Plasma Proteomics and Systemic Tumor Signatures—The >250-fold depletion of high-abundance proteins by SuPrESEC and the identification of a wide range of tumor and systemic proteins (supplemental Fig. S6, Table S1) suggested proteomic characterization of the low M_w subproteome pro-

vided an effective approach to plasma analysis. The capture of the degradome and peptidome, portions of plasma containing fragmented proteins and potential biomarkers, likely contributed to the success of this method (84–86).

The overabundance of tumor-derived proteins in terminal plasma strongly suggested tumor lysis as a dominant mechanism (Figs. 8*A*–8*E*, supplemental S6), a process described in aggressive therapies and lymphoma (87–89). Lysis product overabundance correlated with tumor aggression and higher rates of cell death, most clearly in Eμ-*myc* tumors. A correlation between total protein abundance in the B-cell proteome and overabundance in the plasma was observed, regardless of tumor overexpression (supplemental Fig. S6*G*–S6*I*). Several of these proteins were annotated biomarkers (supplemental Fig. S6*H*) highlighting tumor-lysis products in late-stage, aggressive tumors, as the dominant biomarker signature. It is likely that exosomes and apoptotic blebs also contributed to this signature.

The systemic immune response signature observed for terminal Eμ-*TCL1* plasma suggested that slower tumor development elicited a greater inflammatory response, perhaps because of gradual accumulation, chronic inflammation and a loss of immune regulation (Figs. 8*E*). An anti-tumor immune signature emerged for both models, when deconvoluted to give the "lysis-free" plasma proteome, which suggested several potential systemic biomarkers (Fig. 8*C*, 8*D*).

The contrasting signatures of tumor lysis and immune response in Eμ-*myc* and Eμ-*TCL1* terminal plasma respectively, was reflective of the vastly differing rates of tumor development. However, in both models the signatures were observed, to a lesser extent, in the opposing tumor.

Several systemic signatures were also observed upon integration of the B-cell tumor and plasma proteomes. Overabundance of the carriers of the extracellular matrix component hyaluronan ITIH1–4 (Fig. 8*E*), substantial tumor overexpression of CD168 (HMMR, hyaluronan-mediated motility receptor) (Fig. 3*D*) and links between hyaluronan, inflammation and tumor growth (90) suggest hyaluronan as a component of the B-cell tumor microenvironment. Given their high concentrations in plasma (supplemental Table S1, supplemental Fig. S6*Q*) (37), ITIH proteins hold potential as biomarkers of B-cell tumors and aberrant hyaluronan metabolism and transport. Fibronectin (FN1), recognized in the promotion of cancers (91), was observed as marginally overabundant and inferred to be functional (supplemental Fig. S6*S*). Given the overexpression of FN1-binding integrin β1 on tumors, this may represent another microenvironment signature of pro-oncogenic interactions with B-cell tumors.

Functional biomarker analysis for overabundant plasma proteins with inferred functionality in tumors highlighted S100A6, a previously proposed biomarker (92, 93), and EIF4G1 (supplemental Fig. S6*T*) suggesting candidates for noninvasive testing directly related to tumor function.

Preterminal Eμ-*TCL1* plasma additionally offered several interesting findings, describing a more clinically-relevant time point in tumorigenesis when a leukemia is present, but is otherwise asymptomatic. The observation of overabundant preterminal "30%" Eμ-*TCL1* plasma proteins common to the terminal signature (Fig. 8*F*, supplemental S6*I*, S6*O*, S6*P*) suggested the characterization of progressive, early biomarkers of B-cell tumors. Components of the tumor lysis-free signature describing a systemic immune response were more prevalent, such as Hp and ITIH1. Proteins correlating with tumor progression, traceable to tumor lysis were, however, also present to some extent, suggesting that both lysis and immune signatures offer a source of biomarkers at earlier stages of tumor development. The more detailed evaluation of the multiple stages of tumor progression, of these and other tumor models, could therefore offer considerable insight into the dynamics of biomarker emergence, better informing biomarker discovery and application.

CONCLUDING REMARKS

In conclusion, this study has detailed the protein expression changes present across highly contrasting B-cell tumors, highlighting dominant features of proliferation and growth. Eμ-*myc* tumors demonstrated a specific trend of epigenomic instability and cytoskeletal component underexpression, whereas Eμ-*TCL1* tumors specifically exhibited ER stress, dysregulated signaling, and IL5-driven proliferation. Many specific targets of kinase inhibitors, nucleoside analogues and immunotherapy emerged for each tumor type. Plasma proteomics indicated lysis products as a major late-stage tumor biomarker signature, dominantly in the more aggressive Eμ-*myc* tumors, whereas Eμ-*TCL1* tumor plasma had a dominant signature of an anti-tumor immune response. Integration of plasma and B-cell proteomics data, alongside tumor lysis, highlighted IL5, HMMR/CD168, ITIH proteins, FN1, S100A6, and EIF4G1 as candidate biomarkers for further investigation. These findings reinforce that aggressive, targeted, chemotherapy and immunostimulatory antibodies promise effective means of treating Eμ-*myc* and Eμ-*TCL1* tumors, respectively with the results offering exciting possibilities when combined and integrated with further additional 'omics and functional data. Finally, these findings suggest that global, integrative evaluation of tumors can provide systemic insight into tumor biology not captured by the evaluation of cells or plasma in isolation.

Acknowledgments—We thank Roger Allsopp and Derek Coates for raising funds for Hope for Guernsey for PAT that allowed the purchasing of the FT-MS proteomics platform at the University of Southampton. We would like to acknowledge the Biomedical Research Facility and their staff, the use of the IRIDIS High Performance Computing Facility and associated support services at the University of Southampton, and the PRIDE team in the submission of our data to the PRIDE database. We would also like to thank Cory White for SPIQuE development, Dr. Xunli Zhang for HPLC access and Theo Roumeliotis for proteomics training. Also thanks to Graham Packham for critical feedback on this work.

* This work was supported by an MRC iCASE studentship awarded to P.A.T. and M.S.C. for H.E.J., a supplementary MRC fellowship awarded to H.E.J., and Grants from Bloodwise (10012 and 12050).

[S] This article contains supplemental material.

** To whom correspondence should be addressed: University of Southampton, Southampton General Hospital, Southampton, SO16 6YD, UK. Tel.: 44–2381 208452; Fax: +44 (0) 23 80704061; E-mail: msc@soton.ac.uk.

Conflict of Interest Disclosure: MSC is a retained consultant for Bioinvent and has performed educational and advisory roles for Baxalta. He has received research funding from Roche, Gilead and GSK. PAT is cofounder of Karus Therapeutics, a NED for the Aptamer Group and has performed educational and advisory roles for Abcam, BioRelate, ReactaBiotech and Waters amongst others. He is also Adjunct Professor, Singapore Institute of Immunology, A*Star, Singapore; and Honorary Professor, Department of Histology and Embryology, University of Athens, Greece.

REFERENCES

1. Iversen, U., Iversen, O. H., Bluming, A. Z., Ziegler, J. L., and Kyalwasi, S. (1972) Cell kinetics of African c.ases of Burkitt lymphoma. A preliminary report. *Eur. J. Cancer* **8**, 305–308
2. Molyneux, E. M., Rochford, R., Griffin, B., Newton, R., Jackson, G., Menon, G., Harrison, C. J., Israels, T., and Bailey, S. (2012) Burkitt's lymphoma. *Lancet* **379**, 1234–1244
3. Adams, J. M., Harris, A. W., Pinkert, C. A., Corcoran, L. M., Alexander, W. S., Cory, S., Palmiter, R. D., and Brinster, R. L. (1985) The c-myc oncogene driven by immunoglobulin enhancers induces lymphoid malignancy in transgenic mice. *Nature* **318**, 533–538
4. Dang, C. V., O'Donnell, K. A., Zeller, K. I., Nguyen, T., Osthus, R. C., and Li, F. (2006) The c-Myc target gene network. *Semin. Cancer Biol.* **16**, 253–264
5. Zeller, K. I., Jegga, A. G., Aronow, B. J., O'Donnell, K. A., and Dang, C. V. (2003) An integrated database of genes responsive to the Myc oncogenic transcription factor: identification of direct genomic targets. *Genome Biol.* **4**, R69
6. Blackwell, T. K., Kretzner, L., Blackwood, E. M., Eisenman, R. N., and Weintraub, H. (1990) Sequence-specific DNA binding by the c-Myc protein. *Science* **250**, 1149–1151
7. Nesbit, C. E., Tersak, J. M., and Prochownik, E. V. (1999) MYC oncogenes and human neoplastic disease. *Oncogene* **18**, 3004–3016
8. Harris, A. W., Pinkert, C. A., Crawford, M., Langdon, W. Y., Brinster, R. L., and Adams, J. M. (1988) The E mu-myc transgenic mouse. A model for high-incidence spontaneous lymphoma and leukemia of early B cells. *J. Exp. Med.* **167**, 353–371
9. Mori, S., Rempel, R. E., Chang, J. T., Yao, G., Lagoo, A. S., Potti, A., Bild, A., and Nevins, J. R. (2008) Utilization of pathway signatures to reveal distinct types of B lymphoma in the Emicro-myc model and human diffuse large B-cell lymphoma. *Cancer Res.* **68**, 8525–8534
10. Zhu, D., Qi, C. F., Morse, H. C., 3rd, Janz, S., and Stevenson, F. K. (2005) Deregulated expression of the Myc cellular oncogene drives development of mouse "Burkitt-like" lymphomas from naive B cells. *Blood* **105**, 2135–2137
11. Hallek, M., Cheson, B. D., Catovsky, D., Caligaris-Cappio, F., Dighiero, G., Dohner, H., Hillmen, P., Keating, M. J., Montserrat, E., Rai, K. R., Kipps, T. J., and International Workshop on Chronic Lymphocytic, L. (2008) Guidelines for the diagnosis and treatment of chronic lymphocytic leukemia: a report from the International Workshop on Chronic Lymphocytic Leukemia updating the National Cancer Institute-Working Group 1996 guidelines. *Blood* **111**, 5446–5456
12. Hallek, M., Cheson, B. D., Catovsky, D., Caligaris-Cappio, F., Dighiero, G., Dohner, H., Hillmen, P., Keating, M. J., Montserrat, E., Rai, K. R., and Kipps, T. J. (2008) Guidelines for the diagnosis and treatment of chronic lymphocytic leukemia: a report from the International Workshop on Chronic Lymphocytic Leukemia updating the National Cancer Institute-Working Group 1996 guidelines. *Blood* **111**, 5446–5456
13. Herling, M., Patel, K. A., Khalili, J., Schlette, E., Kobayashi, R., Medeiros, L. J., and Jones, D. (2006) TCL1 shows a regulated expression pattern in chronic lymphocytic leukemia that correlates with molecular subtypes and proliferative state. *Leukemia* **20**, 280–285
14. Kang, S. M., Narducci, M. G., Lazzeri, C., Mongiovi, A. M., Caprini, E., Bresin, A., Martelli, F., Rothstein, J., Croce, C. M., Cooper, M. D., and Russo, G. (2005) Impaired T- and B-cell development in Tcl1-deficient mice. *Blood* **105**, 1288–1294
15. Said, J. W., Hoyer, K. K., French, S. W., Rosenfelt, L., Garcia-Lloret, M., Koh, P. J., Cheng, T. C., Sulur, G. G., Pinkus, G. S., Kuehl, W. M., Rawlings, D. J., Wall, R., and Teitell, M. A. (2001) TCL1 oncogene expression in B cell subsets from lymphoid hyperplasia and distinct classes of B cell lymphoma. *Laboratory Investigation* **81**, 555–564
16. Pekarsky, Y., Koval, A., Hallas, C., Bichi, R., Tresini, M., Malstrom, S., Russo, G., Tsichlis, P., and Croce, C. M. (2000) Tcl1 enhances Akt kinase activity and mediates its nuclear translocation. *Proc. Natl. Acad. Sci. U. S. A.* **97**, 3028–3033
17. Laine, J., Kunstle, G., Obata, T., Sha, M., and Noguchi, M. (2000) The protooncogene TCL1 is an Akt kinase coactivator. *Mol. Cell* **6**, 395–407
18. Bichi, R., Shinton, S. A., Martin, E. S., Koval, A., Calin, G. A., Cesari, R., Russo, G., Hardy, R. R., and Croce, C. M. (2002) Human chronic lymphocytic leukemia modeled in mouse by targeted TCL1 expression. *Proc. Natl. Acad. Sci. U. S. A.* **99**, 6955–6960
19. Johnson, A. J., Lucas, D. M., Muthusamy, N., Smith, L. L., Edwards, R. B., De Lay, M. D., Croce, C. M., Grever, M. R., and Byrd, J. C. (2006) Characterization of the TCL-1 transgenic mouse as a preclinical drug development tool for human chronic lymphocytic leukemia. *Blood* **108**, 1334–1338
20. Pekarsky, Y., Drusco, A., Kumchala, P., Croce, C. M., and Zanesi, N. (2015) The long journey of TCL1 transgenic mice: lessons learned in the last 15 years. *Gene Expr.* **16**, 129–135
21. Simonetti, G., Bertilaccio, M. T., Ghia, P., and Klein, U. (2014) Mouse models in the study of chronic lymphocytic leukemia pathogenesis and therapy. *Blood* **124**, 1010–1019
22. Wilhelm, M., Schlegl, J., Hahne, H., Moghaddas Gholami, A., Lieberenz, M., Savitski, M. M., Ziegler, E., Butzmann, L., Gessulat, S., Marx, H., Mathieson, T., Lemeer, S., Schnatbaum, K., Reimer, U., Wenschuh, H., Mollenhauer, M., Slotta-Huspenina, J., Boese, J. H., Bantscheff, M., Gerstmair, A., Faerber, F., and Kuster, B. (2014) Mass-spectrometry-based draft of the human proteome. *Nature* **509**, 582–587
23. Kim, M. S., Pinto, S. M., Getnet, D., Nirujogi, R. S., Manda, S. S., Chaerkady, R., Madugundu, A. K., Kelkar, D. S., Isserlin, R., Jain, S., Thomas, J. K., Muthusamy, B., Leal-Rojas, P., Kumar, P., Sahasrabuddhe, N. A., Balakrishnan, L., Advani, J., George, B., Renuse, S., Selvan, L. D., Patil, A. H., Nanjappa, V., Radhakrishnan, A., Prasad, S., Subbannayya, T., Raju, R., Kumar, M., Sreenivasamurthy, S. K., Marimuthu, A., Sathe, G. J., Chavan, S., Datta, K. K., Subbannayya, Y., Sahu, A., Yelamanchi, S. D., Jayaram, S., Rajagopalan, P., Sharma, J., Murthy, K. R., Syed, N., Goel, R., Khan, A. A., Ahmad, S., Dey, G., Mudgal, K., Chatterjee, A., Huang, T. C., Zhong, J., Wu, X., Shaw, P. G., Freed, D., Zahari, M. S., Mukherjee, K. K., Shankar, S., Mahadevan, A., Lam, H., Mitchell, C. J., Shankar, S. K., Satishchandra, P., Schroeder, J. T., Sirdeshmukh, R., Maitra, A., Leach, S. D., Drake, C. G., Halushka, M. K., Prasad, T. S., Hruban, R. H., Kerr, C. L., Bader, G. D., Iacobuzio-Donahue, C. A., Gowda, H., and Pandey, A. (2014) A draft map of the human proteome. *Nature* **509**, 575–581
24. Nanjappa, V., Thomas, J. K., Marimuthu, A., Muthusamy, B., Radhakrishnan, A., Sharma, R., Ahmad Khan, A., Balakrishnan, L., Sahasrabuddhe, N. A., Kumar, S., Jhaveri, B. N., Sheth, K. V., Kumar Khatana, R., Shaw, P. G., Srikanth, S. M., Mathur, P. P., Shankar, S., Nagaraja, D., Christopher, R., Mathivanan, S., Raju, R., Sirdeshmukh, R., Chatterjee, A., Simpson, R. J., Harsha, H. C., Pandey, A., and Prasad, T. S. (2014) Plasma Proteome Database as a resource for proteomics research: 2014 update. *Nucleic Acids Res.* **42**, D959–965
25. Keshishian, H., Burgess, M. W., Gillette, M. A., Mertins, P., Clauser, K. R., Mani, D. R., Kuhn, E. W., Farrell, L. A., Gerszten, R. E., and Carr, S. A. (2015) Multiplexed, quantitative workflow for sensitive biomarker discovery in plasma yields novel candidates for early myocardial injury. *Mol. Cell. Proteomics* **14**, 2375–2393
26. Jones, K. A., Kim, P. D., Patel, B. B., Kelsen, S. G., Braverman, A., Swinton, D. J., Gafken, P. R., Jones, L. A., Lane, W. S., Neveu, J. M., Leung, H. C., Shaffer, S. A., Leszyk, J. D., Stanley, B. A., Fox, T. E., Stanley, A., Hall, M. J., Hampel, H., South, C. D., de la Chapelle, A., Burt, R. W., Jones, D. A., Kopelovich, L., and Yeung, A. T. (2013) Immunodepletion plasma proteom-

ics by tripleTOF 5600 and Orbitrap elite/LTQ-Orbitrap Velos/Q exactive mass spectrometers. *J. Proteome Res.* **12**, 4351–4365
27. Patel, B. B., Barrero, C. A., Braverman, A., Kim, P. D., Jones, K. A., Chen, D. E., Bowler, R. P., Merali, S., Kelsen, S. G., and Yeung, A. T. (2012) Assessment of two immunodepletion methods: off-target effects and variations in immunodepletion efficiency may confound plasma proteomics. *J. Proteome Res.* 11, 5947–5958
28. Al-Daghri, N. M., Al-Attas, O. S., Johnston, H. E., Singhania, A., Alokail, M. S., Alkharfy, K. M., Abd-Alrahman, S. H., Sabico, S. L., Roumeliotis, T. I., Manousopoulou-Garbis, A., Townsend, P. A., Woelk, C. H., Chrousos, G. P., and Garbis, S. D. (2014) Whole serum 3D LC-nESI-FTMS quantitative proteomics reveals sexual dimorphism in the milieu interieur of overweight and obese adults. *J. Proteome Res.* **13**, 5094–5105
29. Garbis, S. D., Roumeliotis, T. I., Tyritzis, S. I., Zorpas, K. M., Pavlakis, K., and Constantinides, C. A. (2011) A novel multidimensional protein identification technology approach combining protein size exclusion prefractionation, peptide zwitterion-ion hydrophilic interaction chromatography, and nano-ultraperformance RP chromatography/nESI-MS2 for the in-depth analysis of the serum proteome and phosphoproteome: application to clinical sera derived from humans with benign prostate hyperplasia. *Anal. Chem.* **83**, 708–718
30. Adeghe, A. J., and Cohen, J. (1986) A better method for terminal bleeding of mice. *Lab. Animals* **20**, 70–72
31. Hahne, H., Pachl, F., Ruprecht, B., Maier, S. K., Klaeger, S., Helm, D., Medard, G., Wilm, M., Lemeer, S., and Kuster, B. (2013) DMSO enhances electrospray response, boosting sensitivity of proteomic experiments. *Nat. Methods* **10**, 989–991
32. Vizcaino, J. A., Deutsch, E. W., Wang, R., Csordas, A., Reisinger, F., Rios, D., Dianes, J. A., Sun, Z., Farrah, T., Bandeira, N., Binz, P. A., Xenarios, I., Eisenacher, M., Mayer, G., Gatto, L., Campos, A., Chalkley, R. J., Kraus, H. J., Albar, J. P., Martinez-Bartolome, S., Apweiler, R., Omenn, G. S., Martens, L., Jones, A. R., and Hermjakob, H. (2014) ProteomeXchange provides globally coordinated proteomics data submission and dissemination. *Nat. Biotechnol.* **32**, 223–226
33. Levin, Y. (2011) The role of statistical power analysis in quantitative proteomics. *Proteomics* **11**, 2565–2567
34. Blunt, M. D., Carter, M. J., Larrayoz, M., Smith, L. D., Aguilar-Hernandez, M., Cox, K. L., Tipton, T., Reynolds, M., Murphy, S., Lemm, E., Dias, S., Duncombe, A., Strefford, J. C., Johnson, P. W., Forconi, F., Stevenson, F. K., Packham, G., Cragg, M. S., and Steele, A. J. (2015) The PI3K/mTOR inhibitor PF-04691502 induces apoptosis and inhibits microenvironmental signaling in CLL and the Emicro-TCL1 mouse model. *Blood* **125**, 4032–4041
35. Hussain, K., Hargreaves, C. E., Roghanian, A., Oldham, R. J., Chan, H. T., Mockridge, C. I., Chowdhury, F., Frendeus, B., Harper, K. S., Strefford, J. C., Cragg, M. S., Glennie, M. J., Williams, A. P., and French, R. R. (2015) Upregulation of FcgammaRIIb on monocytes is necessary to promote the superagonist activity of TGN1412. *Blood* **125**, 102–110
36. Ivanov, A., Cragg, M. S., Erenpreisa, J., Emzinsh, D., Lukman, H., and Illidge, T. M. (2003) Endopolyploid cells produced after severe genotoxic damage have the potential to repair DNA double strand breaks. *J. Cell Sci.* **116**, 4095–4106
37. Farrah, T., Deutsch, E. W., Omenn, G. S., Campbell, D. S., Sun, Z., Bletz, J. A., Mallick, P., Katz, J. E., Malmstrom, J., Ossola, R., Watts, J. D., Lin, B., Zhang, H., Moritz, R. L., and Aebersold, R. (2011) A high-confidence human plasma proteome reference set with estimated concentrations in PeptideAtlas. *Mol. Cell. Proteomics* **10**, M110 006353
38. Rounbehler, R. J., Fallahi, M., Yang, C., Steeves, M. A., Li, W., Doherty, J. R., Schaub, F. X., Sanduja, S., Dixon, D. A., Blackshear, P. J., and Cleveland, J. L. (2012) Tristetraprolin impairs myc-induced lymphoma and abolishes the malignant state. *Cell* **150**, 563–574
39. Ow, S. Y., Salim, M., Noirel, J., Evans, C., and Wright, P. C. (2011) Minimising iTRAQ ratio compression through understanding LC-MS elution dependence and high-resolution HILIC fractionation. *Proteomics* **11**, 2341–2346
40. Karp, N. A., Huber, W., Sadowski, P. G., Charles, P. D., Hester, S. V., and Lilley, K. S. (2010) Addressing accuracy and precision issues in iTRAQ quantitation. *Mol. Cell. Proteomics* **9**, 1885–1897
41. Snauwaert, S., Vanhee, S., Goetgeluk, G., Verstichel, G., Van Caeneghem, Y., Velghe, I., Philippe, J., Berneman, Z. N., Plum, J., Taghon, T., Leclercq, G., Thielemans, K., Kerre, T., and Vandekerckhove, B. (2012) RHAMM/HMMR (CD168) is not an ideal target antigen for immunotherapy of acute myeloid leukemia. *Haematologica* **97**, 1539–1547
42. Giannopoulos, K., Li, L., Bojarska-Junak, A., Rolinski, J., Dmoszynska, A., Hus, I., Greiner, J., Renner, C., Dohner, H., and Schmitt, M. (2006) Expression of RHAMM/CD168 and other tumor-associated antigens in patients with B-cell chronic lymphocytic leukemia. *Int. J. Oncol.* **29**, 95–103
43. Szklarczyk, D., Franceschini, A., Wyder, S., Forslund, K., Heller, D., Huerta-Cepas, J., Simonovic, M., Roth, A., Santos, A., Tsafou, K. P., Kuhn, M., Bork, P., Jensen, L. J., and von Mering, C. (2015) STRING v10: protein-protein interaction networks, integrated over the tree of life. *Nucleic Acids Res.* **43**, D447–452
44. Kramer, A., Green, J., Pollard, J., Jr., and Tugendreich, S. (2014) Causal analysis approaches in Ingenuity Pathway Analysis. *Bioinformatics* **30**, 523–530
45. Eom, G. H., Nam, Y. S., Oh, J. G., Choe, N., Min, H. K., Yoo, E. K., Kang, G., Nguyen, V. H., Min, J. J., Kim, J. K., Lee, I. K., Bassel-Duby, R., Olson, E. N., Park, W. J., and Kook, H. (2014) Regulation of acetylation of histone deacetylase 2 by p300/CBP-associated factor/histone deacetylase 5 in the development of cardiac hypertrophy. *Circ. Res.* **114**, 1133–1143
46. Ochs, R. C., and Bagg, A. (2012) Molecular genetic characterization of lymphoma: application to cytology diagnosis. *Diagnostic Cytopathol.* **40**, 542–555
47. Love, C., Sun, Z., Jima, D., Li, G., Zhang, J., Miles, R., Richards, K. L., Dunphy, C. H., Choi, W. W., Srivastava, G., Lugar, P. L., Rizzieri, D. A., Lagoo, A. S., Bernal-Mizrachi, L., Mann, K. P., Flowers, C. R., Naresh, K. N., Evens, A. M., Chadburn, A., Gordon, L. I., Czader, M. B., Gill, J. I., Hsi, E. D., Greenough, A., Moffitt, A. B., McKinney, M., Banerjee, A., Grubor, V., Levy, S., Dunson, D. B., and Dave, S. S. (2012) The genetic landscape of mutations in Burkitt lymphoma. *Nat. Gen.* **44**, 1321–1325
48. Yustein, J. T., Liu, Y. C., Gao, P., Jie, C., Le, A., Vuica-Ross, M., Chng, W. J., Eberhart, C. G., Bergsagel, P. L., and Dang, C. V. (2010) Induction of ectopic Myc target gene JAG2 augments hypoxic growth and tumorigenesis in a human B-cell model. *Proc. Natl. Acad. Sci. U. S. A.* **107**, 3534–3539
49. Xiao, W., Tran, B., Staudt, L. M., and Schmitz, R. (2013) High-throughput RNA sequencing in B-cell lymphomas. *Meth. Mol. Biol.* **971**, 295–312
50. Gygi, S. P., Rochon, Y., Franza, B. R., and Aebersold, R. (1999) Correlation between protein and mRNA abundance in yeast. *Mol. Cell. Biol.* **19**, 1720–1730
51. Vogel, C., and Marcotte, E. M. (2012) Insights into the regulation of protein abundance from proteomic and transcriptomic analyses. *Nat. Rev. Genet.* **13**, 227–232
52. Schwanhausser, B., Busse, D., Li, N., Dittmar, G., Schuchhardt, J., Wolf, J., Chen, W., and Selbach, M. (2011) Global quantification of mammalian gene expression control. *Nature* **473**, 337–342
53. Tabarkiewicz, J., and Giannopoulos, K. (2010) Definition of a target for immunotherapy and results of the first Peptide vaccination study in chronic lymphocytic leukemia. *Transplant Proc.* **42**, 3293–3296
54. Solana, R., Romero, J., Alonso, C., and Pena, J. (1992) MHC class I antigen expression is inversely related with tumor malignancy and ras oncogene product (p21ras) levels in human breast tumors. *Invasion Metastasis* **12**, 210–217
55. Paulson, K. G., Tegeder, A., Willmes, C., Iyer, J. G., Afanasiev, O. K., Schrama, D., Koba, S., Thibodeau, R., Nagase, K., Simonson, W. T., Seo, A., Koelle, D. M., Madeleine, M., Bhatia, S., Nakajima, H., Sano, S., Hardwick, J. S., Disis, M. L., Cleary, M. A., Becker, J. C., and Nghiem, P. (2014) Downregulation of MHC-I expression is prevalent but reversible in Merkel cell carcinoma. *Cancer Immunol. Res.* **2**, 1071–1079
56. Gaudet, F., Hodgson, J. G., Eden, A., Jackson-Grusby, L., Dausman, J., Gray, J. W., Leonhardt, H., and Jaenisch, R. (2003) Induction of tumors in mice by genomic hypomethylation. *Science* **300**, 489–492
57. Hopp, L., Nersisyan, L., Loffler-Wirth, H., Arakelyan, A., and Binder, H. (2015) Epigenetic heterogeneity of B-Cell lymphoma: chromatin modifiers. *Genes* **6**, 1076–1112
58. Li, S., Garrett-Bakelman, F. E., Chung, S. S., Sanders, M. A., Hricik, T., Rapaport, F., Patel, J., Dillon, R., Vijay, P., Brown, A. L., Perl, A. E., Cannon, J., Bullinger, L., Luger, S., Becker, M., Lewis, I. D., To, L. B., Delwel, R., Lowenberg, B., Dohner, H., Dohner, K., Guzman, M. L., Hassane, D. C., Roboz, G. J., Grimwade, D., Valk, P. J., D'Andrea, R. J., Carroll, M., Park, C. Y., Neuberg, D., Levine, R., Melnick, A. M., and Mason, C. E. (2016) Distinct evolution and dynamics of epigenetic

and genetic heterogeneity in acute myeloid leukemia. *Nat. Med.* **22**, 792–799
59. Pollard, T. D., and Borisy, G. G. (2003) Cellular motility driven by assembly and disassembly of actin filaments. *Cell* **112**, 453–465
60. Foger, N., Rangell, L., Danilenko, D. M., and Chan, A. C. (2006) Requirement for coronin 1 in T lymphocyte trafficking and cellular homeostasis. *Science* **313**, 839–842
61. Haraldsson, M. K., Louis-Dit-Sully, C. A., Lawson, B. R., Sternik, G., Santiago-Raber, M. L., Gascoigne, N. R., Theofilopoulos, A. N., and Kono, D. H. (2008) The lupus-related Lmb3 locus contains a disease-suppressing Coronin-1A gene mutation. *Immunity* **28**, 40–51
62. Al Tanoury, Z., Schaffner-Reckinger, E., Halavatyi, A., Hoffmann, C., Moes, M., Hadzic, E., Catillon, M., Yatskou, M., and Friederich, E. (2010) Quantitative kinetic study of the actin-bundling protein L-plastin and of its impact on actin turn-over. *PLoS One* **5**, e9210
63. Todd, E. M., Deady, L. E., and Morley, S. C. (2011) The actin-bundling protein L-plastin is essential for marginal zone B cell development. *J. Immunol.* **187**, 3015–3025
64. Todd, E. M., Deady, L. E., and Morley, S. C. (2013) Intrinsic T- and B-cell defects impair T-cell-dependent antibody responses in mice lacking the actin-bundling protein L-plastin. *Eur. J. Immunol.* **43**, 1735–1744
65. Parikh, S. S., Litherland, S. A., Clare-Salzler, M. J., Li, W., Gulig, P. A., and Southwick, F. S. (2003) CapG(-/-) mice have specific host defense defects that render them more susceptible than CapG(+/+) mice to Listeria monocytogenes infection but not to Salmonella enterica serovar Typhimurium infection. *Infect. Immun.* **71**, 6582–6590
66. Foran, E., McWilliam, P., Kelleher, D., Croke, D. T., and Long, A. (2006) The leukocyte protein L-plastin induces proliferation, invasion and loss of E-cadherin expression in colon cancer cells. *Int. J. Cancer.* **118**, 2098–2104
67. Glaser, J., Neumann, M. H., Mei, Q., Betz, B., Seier, N., Beyer, I., Fehm, T., Neubauer, H., Niederacher, D., and Fleisch, M. C. (2014) Macrophage capping protein CapG is a putative oncogene involved in migration and invasiveness in ovarian carcinoma. *Biomed. Res. Int.* 2014, 379847
68. Shankar, J., Messenberg, A., Chan, J., Underhill, T. M., Foster, L. J., and Nabi, I. R. (2010) Pseudopodial actin dynamics control epithelial-mesenchymal transition in metastatic cancer cells. *Cancer Res.* **70**, 3780–3790
69. Kriss, C. L., Pinilla-Ibarz, J. A., Mailloux, A. W., Powers, J. J., Tang, C. H., Kang, C. W., Zanesi, N., Epling-Burnette, P. K., Sotomayor, E. M., Croce, C. M., Del Valle, J. R., and Hu, C. C. (2012) Overexpression of TCL1 activates the endoplasmic reticulum stress response: a novel mechanism of leukemic progression in mice. *Blood* **120**, 1027–1038
70. Iacovelli, S., Hug, E., Bennardo, S., Duehren-von Minden, M., Gobessi, S., Rinaldi, A., Suljagic, M., Bilbao, D., Bolasco, G., Eckl-Dorna, J., Niederberger, V., Autore, F., Sica, S., Laurenti, L., Wang, H., Cornall, R. J., Clarke, S. H., Croce, C. M., Bertoni, F., Jumaa, H., and Efremov, D. G. (2015) Two types of BCR interactions are positively selected during leukemia development in the Emu-TCL1 transgenic mouse model of CLL. *Blood* **125**, 1578–1588
71. Slavin, S., and Strober, S. (1978) Spontaneous murine B-cell leukaemia. *Nature* **272**, 624–626
72. O'Garra, A., Barbis, D., Wu, J., Hodgkin, P. D., Abrams, J., and Howard, M. (1989) The BCL1 B lymphoma responds to IL-4, IL-5, and GM-CSF. *Cell Immunol.* **123**, 189–200
73. Lohoff, M., Sommer, F., and Rollinghoff, M. (1989) Suppressive effect of interferon-gamma on the BCL1 cell-dependent interleukin 5 bioassay. *Eur. J. Immunol.* **19**, 1327–1329
74. Lasky, J. L., and Thorbecke, G. J. (1989) Characterization and growth factor requirements of SJL lymphomas. II. Interleukin 5 dependence of the in vitro cell line, cRCS-X, and influence of other cytokines. *Eur. J. Immunol.* **19**, 365–371
75. Wen, X., Zhang, D., Kikuchi, Y., Jiang, Y., Nakamura, K., Xiu, Y., Tsurui, H., Takahashi, K., Abe, M., Ohtsuji, M., Nishimura, H., Takatsu, K., Shirai, T., and Hirose, S. (2004) Transgene-mediated hyper-expression of IL-5 inhibits autoimmune disease but increases the risk of B cell chronic lymphocytic leukemia in a model of murine lupus. *Eur. J. Immunol.* 34, 2740–2749
76. Sato, S., Katagiri, T., Takaki, S., Kikuchi, Y., Hitoshi, Y., Yonehara, S., Tsukada, S., Kitamura, D., Watanabe, T., Witte, O., and Takatsu, K. (1994) IL-5 receptor-mediated tyrosine phosphorylation of SH2/SH3-containing proteins and activation of Bruton's tyrosine and Janus 2 kinases. *J. Exp. Med.* **180**, 2101–2111
77. Coffer, P. J., Schweizer, R. C., Dubois, G. R., Maikoe, T., Lammers, J. W., and Koenderman, L. (1998) Analysis of signal transduction pathways in human eosinophils activated by chemoattractants and the T-helper 2-derived cytokines interleukin-4 and interleukin-5. *Blood* **91**, 2547–2557
78. Adachi, T., and Alam, R. (1998) The mechanism of IL-5 signal transduction. *Am. J. Physiol.* **275**, C623–633
79. Wetzel, G. D. (1989) Interleukin 5 regulation of peritoneal Ly-1 B lymphocyte proliferation, differentiation and autoantibody secretion. *Eur. J. Immunol.* **19**, 1701–1707
80. Sanderson, C. J. (1988) Interleukin-5: an eosinophil growth and activation factor. *Dev. Biol. Stand.* **69**, 23–29
81. Kopf, M., Brombacher, F., Hodgkin, P. D., Ramsay, A. J., Milbourne, E. A., Dai, W. J., Ovington, K. S., Behm, C. A., Kohler, G., Young, I. G., and Matthaei, K. I. (1996) IL-5-deficient mice have a developmental defect in CD5+ B-1 cells and lack eosinophilia but have normal antibody and cytotoxic T cell responses. *Immunity* **4**, 15–24
82. Clutterbuck, E., Shields, J. G., Gordon, J., Smith, S. H., Boyd, A., Callard, R. E., Campbell, H. D., Young, I. G., and Sanderson, C. J. (1987) Recombinant human interleukin 5 is an eosinophil differentiation factor but has no activity in standard human B cell growth factor assays. *Eur. J. Immunol.* **17**, 1743–1750
83. Mainou-Fowler, T., and Prentice, A. G. (1996) Modulation of apoptosis with cytokines in B-cell chronic lymphocytic leukaemia. *Leukemia Lymphoma* **21**, 369–377
84. van Winden, A. W., van den Broek, I., Gast, M. C., Engwegen, J. Y., Sparidans, R. W., van Dulken, E. J., Depla, A. C., Cats, A., Schellens, J. H., Peeters, P. H., Beijnen, J. H., and van Gils, C. H. (2010) Serum degradome markers for the detection of breast cancer. *J. Proteome Res.* **9**, 3781–3788
85. Karczmarski, J., Rubel, T., Mikula, M., Wolski, J., Rutkowski, A., Zagorowicz, E., Dadlez, M., and Ostrowski, J. (2013) Pre-analytical-related variability influencing serum peptide profiles demonstrated in a mass spectrometry-based search for colorectal and prostate cancer biomarkers. *Acta Biochim. Pol.* **60**, 417–425
86. Yang, J., Yang, J., Gao, Y., Zhao, L., Liu, L., Qin, Y., Wang, X., Song, T., and Huang, C. (2014) Identification of potential serum proteomic biomarkers for clear cell renal cell carcinoma. *PLoS One* **9**, e111364
87. Davidson, M. B., Thakkar, S., Hix, J. K., Bhandarkar, N. D., Wong, A., and Schreiber, M. J. (2004) Pathophysiology, clinical consequences, and treatment of tumor lysis syndrome. *Am. J. Med.* **116**, 546–554
88. Wossmann, W., Schrappe, M., Meyer, U., Zimmermann, M., and Reiter, A. (2003) Incidence of tumor lysis syndrome in children with advanced stage Burkitt's lymphoma/leukemia before and after introduction of prophylactic use of urate oxidase. *Ann. Hematol.* **82**, 160–165
89. Otrock, Z. K., Hatoum, H. A., and Salem, Z. M. (2008) Acute tumor lysis syndrome after rituximab administration in Burkitt's lymphoma. *Intern. Emerg. Med.* **3**, 161–163
90. Misra, S., Hascall, V. C., Markwald, R. R., and Ghatak, S. (2015) Interactions between hyaluronan and its receptors (CD44, RHAMM) Regulate the activities of inflammation and cancer. *Front. Immunol.* **6**, 201
91. Sponziello, M., Rosignolo, F., Celano, M., Maggisano, V., Pecce, V., De Rose, R. F., Lombardo, G. E., Durante, C., Filetti, S., Damante, G., Russo, D., and Bulotta, S. (2016) Fibronectin-1 expression is increased in aggressive thyroid cancer and favors the migration and invasion of cancer cells. *Mol. Cell. Endocrinol.* **431**, 123–132
92. Zhang, J., Zhang, K., Jiang, X., and Zhang, J. (2014) S100A6 as a potential serum prognostic biomarker and therapeutic target in gastric cancer. *Dig. Dis. Sci.* **59**, 2136–2144
93. Nishi, M., Matsumoto, K., Kobayashi, M., Yanagita, K., Matsumoto, T., Nagashio, R., Ishii, D., Fujita, T., Sato, Y., and Iwamura, M. (2014) Serum expression of S100A6 is a potential detection marker in patients with urothelial carcinoma in the urinary bladder. *Biomed. Res.* 35, 351–356
94. Supek, F., Bosnjak, M., Skunca, N., and Smuc, T. (2011) REVIGO summarizes and visualizes long lists of gene ontology terms. *PLoS One* **6**, e21800